

Kollonige, Debra E., Anne M. Thompson, Miroslav Josipovic, Maria Tzortziou, Johan P. Beukes, Roelof Burger, Douglas K. Martins, Pieter G. van Zyl, Ville Vakkari, and Lauri Laakso. "OMI Satellite and Ground-Based Pandora Observations and Their Application to Surface NO₂ Estimations at Terrestrial and Marine Sites." *Journal of Geophysical Research: Atmospheres* 123, no. 2 (2018): 1441–59.

<https://doi.org/10.1002/2017JD026518>.

<https://agupubs.onlinelibrary.wiley.com/doi/10.1002/2017JD026518>

Access to this work was provided by the University of Maryland, Baltimore County (UMBC) ScholarWorks@UMBC digital repository on the Maryland Shared Open Access (MD-SOAR) platform.

Please provide feedback

Please support the ScholarWorks@UMBC repository by emailing scholarworks-group@umbc.edu and telling us what having access to this work means to you and why it's important to you. Thank you.

RESEARCH ARTICLE

10.1002/2017JD026518

Key Points:

- This analysis estimates surface NO₂ from total column Pandora and OMI observations over South Africa and over North Atlantic Ocean
- Ground and satellite surface NO₂ estimations over land are more similar as compared to over ocean with cleaner air
- Planetary boundary layer height and weather conditions impact the performance of this method in both terrestrial and marine environments

Correspondence to:

D. E. Kollonige,
dewk13@umd.edu

Citation:

Kollonige, D. E., Thompson, A. M., Josipovic, M., Tzortziou, M., Beukes, J. P., Burger, R., ... Laakso, L. (2018). OMI satellite and ground-based Pandora observations and their application to surface NO₂ estimations at terrestrial and marine sites. *Journal of Geophysical Research: Atmospheres*, 123, 1441–1459. <https://doi.org/10.1002/2017JD026518>

Received 17 JAN 2017

Accepted 4 NOV 2017

Accepted article online 8 NOV 2017

Published online 29 JAN 2018

OMI Satellite and Ground-Based Pandora Observations and Their Application to Surface NO₂ Estimations at Terrestrial and Marine Sites

Debra E. Kollonige^{1,2} , Anne M. Thompson^{2,3,4} , Miroslav Josipovic⁴, Maria Tzortziou^{2,5}, Johan P. Beukes⁴ , Roelof Burger⁴, Douglas K. Martins⁶ , Pieter G. van Zyl⁴ , Ville Vakkari⁷, and Lauri Laakso^{4,7}

¹Earth System Science Interdisciplinary Center (ESSIC), University of Maryland, College Park, MD, USA, ²NASA/Goddard, Greenbelt, MD, USA, ³Department of Meteorology, The Pennsylvania State University, University Park, PA, USA, ⁴Unit for Environmental Sciences and Management, North-West University, Potchefstroom, South Africa, ⁵Department of Earth and Atmospheric Science, City University of New York, New York, NY, USA, ⁶FLIR Systems, Inc, West Lafayette, IN, USA, ⁷Finnish Meteorological Institute, Helsinki, Finland

Abstract The Pandora spectrometer that uses direct-Sun measurements to derive total column amounts of gases provides an approach for (1) validation of satellite instruments and (2) monitoring of total column (TC) ozone (O₃) and nitrogen dioxide (NO₂). We use for the first time Pandora and Ozone Monitoring Instrument (OMI) observations to estimate surface NO₂ over marine and terrestrial sites downwind of urban pollution and compared with in situ measurements during campaigns in contrasting regions: (1) the South African Highveld (at Welgegund, 26°34'10"S, 26°56'21"E, 1,480 m asl, ~120 km southwest of the Johannesburg-Pretoria megacity) and (2) shipboard U.S. mid-Atlantic coast during the 2014 Deposition of Atmospheric Nitrogen to Coastal Ecosystems (DANCE) cruise. In both cases, there were no local NO_x sources but intermittent regional pollution influences. For TC NO₂, OMI and Pandora difference is ~20%, with Pandora higher most times. Surface NO₂ values estimated from OMI and Pandora columns are compared to in situ NO₂ for both locations. For Welgegund, the planetary boundary layer (PBL) height, used in converting column to surface NO₂ value, has been estimated by three methods: co-located Atmospheric Infrared Sounder (AIRS) observations; a model simulation; and radiosonde data from Irene, 150 km northeast of the site. AIRS PBL heights agree within 10% of radiosonde-derived values. Absolute differences between Pandora- and OMI-estimated surface NO₂ and the in situ data are better at the terrestrial site (~0.5 ppbv and ~1 ppbv or greater, respectively) than under clean marine air conditions, with differences usually >3 ppbv. Cloud cover and PBL variability influence these estimations.

1. Introduction

Satellite remote sensing measurements of trace gases in the atmosphere are a valuable tool for atmospheric chemistry and pollution research by providing synoptic atmospheric observations over a large domain including over ocean. They can supplement regional air pollution monitoring networks (Brauer et al., 2012; He et al., 2013; van Donkelaar et al., 2010). Ground remote sensing measurements support validation of new measurements that focus on North American (Tropospheric Emissions: Monitoring of Pollution (TEMPO; Chance et al., 2013; Fishman et al., 2012; Zoogman et al., 2017)), East Asian (Geo-stationary Environmental Monitoring Spectrometer (GEMS; Kim, 2012)), European and North African (Sentinel-4 (Ingmann et al., 2012)), and global (Tropospheric Monitoring Instrument on Sentinel 5 Precursor (TROPOMI; Loyola et al., 2017) missions. Satellite observations of tropospheric NO₂ column abundance have been conducted since 1995 (Burrows et al., 1999) and are well suited for inferring NO_x emissions (Chai et al., 2009; Lamsal et al., 2011; Lu & Streets, 2012; Streets et al., 2013) and monitoring air pollution across large spatiotemporal scales (Beirle et al., 2011; Boersma et al., 2008; Duncan et al., 2010, 2013, 2014, 2016; Fishman et al., 2008; Hilboll et al., 2013; Kim et al., 2006; Lamsal et al., 2015; Martin, 2008; Russell et al., 2012). However, high-resolution ground-measured NO₂ column abundances often show strong temporal and spatial variability beyond the capability of current satellite observations. These data are essential for understanding the influence of various NO_x sources on local and regional pollution episodes in urban and coastal ecosystems (Herman et al., 2009; Reed et al., 2015; Tzortziou et al., 2015).

The Ozone Monitoring Instrument (OMI; Boersma et al., 2002; Bucsela et al., 2006) on board the Aura satellite and the ground-based Pandora instrument (Herman et al., 2009) derive the total amount of NO₂, among other chemical species, in a vertical column of air through a retrieval algorithm. However, it is a challenge to relate total column (TC) observations to ambient surface volume mixing ratios. For example, one difficulty comes from accounting for variability in the planetary boundary layer (PBL). Because tropospheric NO_x has a relatively short lifetime of several hours up to a few days, the largest concentrations of NO₂ are measured in the boundary layer close to emission sources.

Multiple methods can relate the column retrieved abundances to surface concentrations. Boersma et al. (2009) used surface NO₂ data to derive a boundary-layer column to show how OMI can capture intraday variability caused by diurnal variation of NO₂. Lamsal et al. (2008, 2010) showed that ground-level NO₂ concentrations obtained from OMI simulated with a chemical transport model agree well with corrected in situ measurements in the U.S. and Canada. Similar studies (e.g., Halla et al., 2011; Lee et al., 2011; Leigh et al., 2007; Luo et al., 2012; Petritoli et al., 2004; Peters et al., 2012), comparing satellite or ground-retrieved columns to surface measurements, have utilized complex chemical transport models and/or large averaging times (weekly, seasonal, or annual) that effectively average out the influence of PBL variability. These methods are often inadequate for interpreting health-related NO₂ fluctuations that occur on the order of hours. Knepp et al. (2015) first estimated surface mixing ratios of daily NO₂ with TC NO₂ measurements from a ground-based Pandora spectrometer at a rural and an urban site in the U.S., scaling column concentrations by the boundary layer height. Similarly, Flynn et al. (2014) expanded this study to include several ground sites from the DISCOVER-AQ MD 2011 campaign ranging from suburban (Beltsville) to rural (Aldino) and found the degree of correlation ranging from $R^2 = 0.29$ to 0.01 , respectively, between in situ and column NO₂ from Pandora instruments. Here we adapt the Knepp et al. (2015) method (referred to as Knepp–Kollonige method below) to estimate surface NO₂ concentration with ground- and satellite-based TC observations taken over marine and terrestrial sites downwind of urban pollution when local measurements of the boundary layer height are not available. Rather than using a modeled PBL height, the Knepp–Kollonige method employs for the first time satellite observations of the PBL height when estimating surface NO₂ concentrations.

The objective of this study is to evaluate the first application of the Knepp–Kollonige method on TC NO₂ measurements. Both a marine (along the U.S. East Coast in the Atlantic Ocean) and a terrestrial (Welgegend measurement site that is ~120 km from the Johannesburg–Pretoria (J-P) megacity, South Africa) environment were selected for this evaluation. Surface concentrations of NO₂ (expressed in volume mixing ratios) measured by ground-level trace gas analyzers at the locations are compared to estimated volume mixing ratios obtained from tropospheric vertical column densities retrieved by (a) coincidental, co-located vertical ground-level Pandora measurements and (b) close overpasses of the OMI instrument aboard the NASA Aura satellite. The height of the PBL, a key variable in this method of estimation for scaling the TC NO₂ measurements, is derived from three different approaches, depending on the site and available data: observations from radiosonde launches at the Irene weather station (150 km northeast of Welgegend); co-located Atmospheric Infrared Sounder (AIRS) observations; and a model simulation. Case studies are presented to demonstrate the strengths and weaknesses of this method over each locale and are meant as a prototype for TROPOMI and upcoming geostationary satellite data sets.

2. Data and Methods of Analysis

2.1. Site Locations and In Situ Measurements

Two locations with separate measurement campaigns were selected for the evaluation of the Knepp–Kollonige method for estimating surface NO₂ concentrations from TC NO₂ abundances. The results are compared to available in situ gas analyzer measurements described in the following sections and Table 1.

2.1.1. Welgegend, South Africa Campaign

A prominent NO₂ “hotspot” observed in remote sensing maps derived from satellite observations is present over the South African Mpumalanga Highveld (Duncan et al., 2016; Lourens et al., 2011, 2012) with a similar intensity to other major regional pollution “hotspots,” such as eastern China. This anomaly is attributed to the presence of 15 coal-fired power stations and a number of metallurgical smelters, as well as a large petrochemical industry. In addition to the well-known NO₂ “hotspot,” there are also widespread regional sources, including traffic, biomass burning, and informal settlements with extensive coal and biofuel use,

Table 1*Summary of Ground Instruments at Welgegund, South Africa, Site^a and on Board the Research Vessel Hugh R. Sharp in the North Atlantic During DANCE^b*

Campaign/site name	Location (lat, lon)	Instrument	Data	Time resolution for analysis
Welgegund, South Africa	26°34'S, 26°56'E	Teledyne AU 200 gas analyzer	NO detected by chemiluminescence w/ O ₃ , NO ₂ = NO _x - NO	15 min and 1 h
		Environnement s.a.41M	O ₃ concentration	15 min
		Rotronic MP 101A	Temperature, relative humidity	15 min and 1 h
		Vector A101ML, Vector W200P	Wind direction and speed	15 min and 1 h
		Vaisala QMR102	Precipitation	1 h
DANCE, North Atlantic Ocean	35–39°N, 72–75°W	Pandora (#8) spectrometer ^c	Total column NO ₂	15 min and 1 h
		Aerodyne CAPS NO ₂	NO ₂ concentration	15 min
		—	Temperature, relative humidity	15 min
		Pandora (#24) spectrometer ^c	Total column NO ₂	15 min and 1 h

^aA full list of gas, aerosol, and ecosystem observations at Welgegund is available at www.welgegund.org. ^bMeasurements described in further detail in Petäjä et al. (2013) and Tiitta et al. (2014). Martins et al. (2016) describes in situ ship measurements from DANCE. ^cInstrument from Sci-Globe.

as well as large industrial point sources from metallurgical, mining, and petrochemical operations (Freiman & Piketh, 2003; Laakso et al., 2008, 2012; Venter et al., 2012, 2016). The plumes originating in the Highveld typically mix down to ground level only under very unstable conditions. For example, Balashov et al. (2014) reported relatively low NO_x surface concentrations over the Highveld with no significant NO₂ trend. Duncan et al. (2016), using 10 years of satellite observations, discovered regions of both increasing and decreasing trends in NO₂ over the South African Highveld depending on proximity to sources. With the troposphere usually well stratified (Newell et al., 1999), elevated layers of accumulated pollutants are common over southern Africa (Cosijn & Tyson, 1996; Freiman & Tyson, 2000; Garstang et al., 1996; Giannakaki et al., 2015).

The Welgegund measurement site (26°34'10"S, 26°56'21"E, 1,480 m above sea level) is located approximately 25 km northwest of Potchefstroom (Figure 1, red star, and Figure 2, magenta triangle) and 100 km southwest of the J-P megacity with no significant local pollution sources (Beukes et al., 2013; Booyens et al., 2015; Jaars et al., 2014, 2016; Tiitta et al., 2014; Vakkari et al., 2014). Welgegund is frequently impacted by air masses from a number of source regions including J-P (Jaars et al., 2014; Tiitta et al., 2014), the industrialized Mpumalanga Highveld, the Vaal Triangle to the southeast, known for its metallurgical and petrochemical processing facilities, and the Bushveld Igneous Complex (Venter et al., 2012) with additional mining and metallurgical activities to the northeast (Figure 1). Air masses, passing over the regional background from the west of Welgegund, are relatively clean during the wet season (South African summer, but extends November–April) with no significant point sources (Jaars et al., 2014; Tiitta et al., 2014). During the South African winter months and dry and biomass burning seasons (May–October), limited fire pollution originates from this sector due to its aridity and low biofuel load (Vakkari et al., 2014).

Surface measurements at Welgegund are described in previous studies starting with a mobile atmospheric monitoring trailer in Petäjä et al. (2013) and the permanent placement of instruments at the site in May 2010 in Tiitta et al. (2014) and Beukes et al. (2015). Table 1 summarizes the primary trace gases (O₃ and NO_x) and meteorological parameters from 25 January to 15 March 2011 that were used in this study. Temperature, relative humidity, and precipitation are recorded every minute. The trace gas instruments share a Teflon (polytetrafluoroethylene) sampling line and record measurements at 1 min intervals.

A Teledyne 200 AU gas analyzer detects NO by chemiluminescence after reaction with O₃ and records NO and NO_x measurements. Nitrogen dioxide is determined by conversion to NO through a reduction reaction with molybdenum and subtracting NO from the sum. However, this gas analyzer also converts other reactive, oxidized nitrogen species, NO₂ (HNO₃, PAN, and other organic nitrates), and can cause overestimations of NO_x (and thus NO₂) ranging between ~17% to greater than 50% (Dunlea et al., 2007; Grosjean & Harrison, 1985; Steinbacher et al., 2007). For the time period studied, the in situ NO₂ gives the upper limit of the NO₂ at surface, but due to the abovementioned issue, the actual NO₂ concentration can be up to 50% less. We adopted an uncertainty of ~50% for this type of gas analyzer NO₂ measurements.

The Welgegund instruments are maintained weekly and calibrated every 3 months. Any possible drift in instrument response between calibration checks is corrected for in the quality-controlled data according

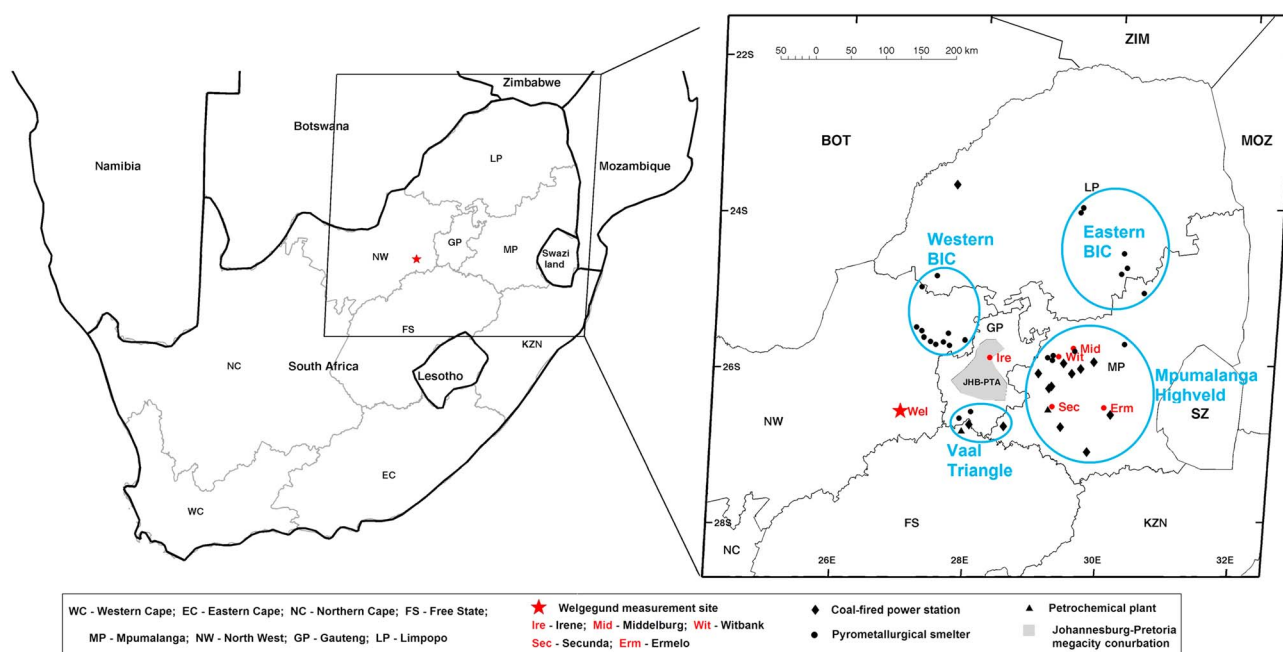


Figure 1. Map of prospective sources of pollution influential on the local air quality of Welgegend site (red star) in South Africa. Irene (red filled circle, Ire), the weather station where radiosondes were launched, is located in the northern area of J-P megacity and 150 km northeast of Welgegend.

to Laakso et al. (2008). All surface data were quality controlled and then averaged over 15 min intervals for comparison to the remotely sensed observations. During this time period, cloud cover and precipitation (strongly influenced by the SA Highveld wet season prevalent in late spring, summer, and early autumn) were highly influential on local air photochemistry. As a result of poor (cloudy/rainy) weather conditions at the station, only 22 days of observations were used between 25 January and 15 March 2011. This time period of observation was a campaign of opportunity and specific to the Fulbright Award afforded to A. M. Thompson (January–April 2011), which only included the wet season for the Welgegend site. This analysis is a demonstration of the application of measurements taken at Welgegend through the limited time period of the Fulbright Award.

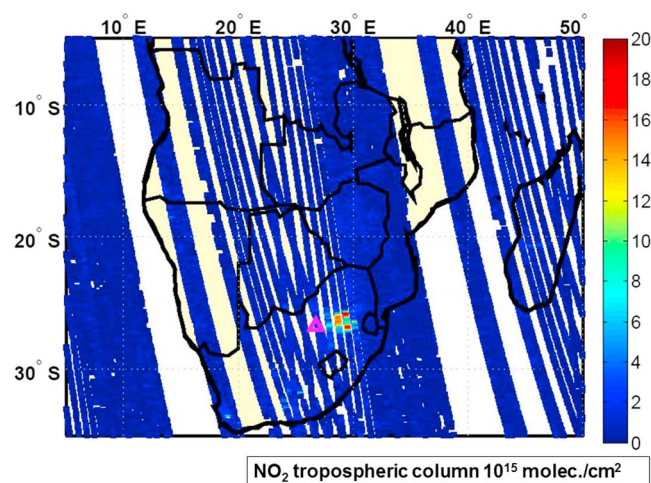


Figure 2. OMI mean tropospheric column NO_2 from OMNO2 version 3 L2 data on 10 March 2011 focused on South Africa between $\sim 15^\circ\text{E}$ – 35°E and 20°S – 35°S , where NO_2 sources are east of Welgegend (magenta triangle) including the Johannesburg–Pretoria megacity, Vaal Triangle, Mpumalanga Highveld, and Bushveld igneous complexes (all indicated in Figure 1) and visible as a hotspot column concentration $> 15 \times 10^{15} \text{ molec./cm}^2$.

2.1.2. North Atlantic Ocean, DANCE Campaign

The Deposition of Atmospheric Nitrogen to Coastal Ecosystems (DANCE) campaign encompassed the area of 34°N – 39°N , 71°W – 76°W (Figure 3) in the North Atlantic Ocean off the mid-Atlantic coast on 29 July to 15 August 2014 where trace gas and meteorological measurements were collected on board the Research Vessel *Hugh R. Sharp*. Leaving from Lewes, Delaware (38.79°N , 75.15°W ; magenta triangle in Figures 3a and 3b), the ship targeted semipermanent anticyclonic eddies at $\sim 38.35^\circ\text{N}$, 72.56°W and $\sim 35.64^\circ\text{N}$, 72.16°W (black solid line traces ship track in Figures 3a and 3b). Due to the scarcity of atmospheric measurements offshore, this data set is important for understanding (1) atmospheric deposition, which influences marine ecosystems (Reay et al., 2008), and (2) any biases between TC trace gas abundances from remote sensors and in situ instruments over open ocean, which impact retrievals of other constituents such as ocean color (Fishman et al., 2012). Figure 3 is an example of the daily OMI NO_2 tropospheric column abundances observed over the Atlantic Ocean during the main pollution event observed over open water on 5–6 August 2014.

Martins et al. (2016) detail the DANCE onboard ship measurements including in situ NO_2 used in this analysis (see also Table 1). Nitrogen dioxide data collected with an Aerodyne CAPS NO_2 instrument was

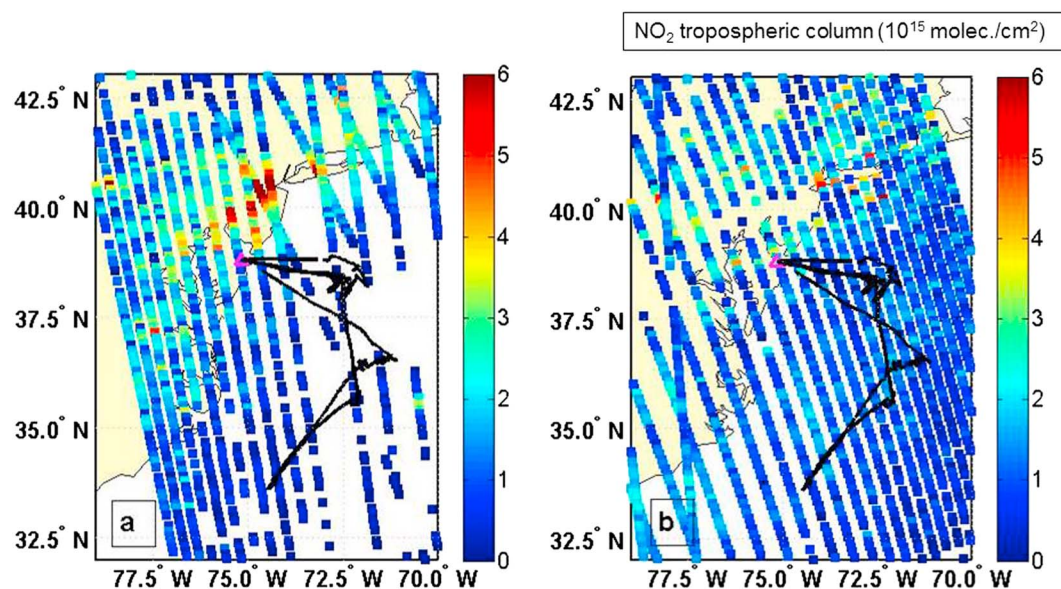


Figure 3. OMI mean tropospheric column NO_2 from OMNO2 version 3 L2 data on (a) 5 August 2014 and (b) 6 August 2014 over the Atlantic Ocean during the DANCE campaign when highest NO_2 levels were observed. The ship track throughout the campaign is denoted by the black solid line, and the magenta triangle is the port of Lewes, DE, where the research vessel departed.

calibrated with an uncertainty of 5%. The in situ measurements were filtered to remove influences from the ship's exhaust because of the placement of the inlet port side. TC NO_2 measurements from a Pandora instrument on board the ship are described in Martins et al. (2016) and the following section.

2.2. Total Column Observations of Nitrogen Dioxide

Co-located total column observations of NO_2 retrieved from a Pandora spectrometer at each site (Table 1) and OMI on board the Aura satellite were selected for this analysis (Table 2). All TC NO_2 observations and their respective surface estimations derived from the Knepp–Kollonige method were compared to each other here. Additionally, Martins et al. (2016) showed direct comparisons between TC NO_2 and in situ surface measurements of NO_2 during the DANCE campaign.

2.2.1. Pandora

At the Welgegund site during 25 January to 15 March 2011, the Sun-only Pandora (280–500 nm) detector, mounted on a computer-controlled Sun tracker, was installed temporarily to retrieve total column O_3 and NO_2 densities approximately every 2 min using direct Sun irradiances. Herman et al. (2009) provides a detailed technical characterization of Pandora, and it is briefly described here. The instrument has a 1.6° field of view and spectral resolution of 0.6 nm. Uncertainties in ambient temperature, absorption cross sections, and cloud cover introduce uncertainties into the Pandora TC NO_2 retrievals and are accounted for in the instrument's retrieval algorithm described in Herman et al. (2009) and more recently in Tzortziou et al. (2012, 2015).

During DANCE, a ship-based direct-Sun Pandora spectrometer was mounted on top of the bridge in front of the ship's exhaust to avoid contamination. TC NO_2 and O_3 were similarly retrieved with data collected on 16 out of 17 days of operation. Further data and instrumentation details are outlined in Martins et al. (2016), including analysis of the influence of the ship's plume on these TC measurements.

Table 2
Summary of Satellite Remote Sensing Observations Used for Case Study Analysis

Instrument	Data	Time resolution for analysis
Aura OMI	Total, stratospheric, and tropospheric column NO_2 , and cloud fraction	1–2 obs per day
Aqua AIRS	Planetary boundary layer top	1–2 obs per day

Validation studies with other ground-based instruments revealed that Pandora total vertical column NO₂ densities compared well with their retrievals. For example, a Fourier transform ultraviolet spectrometer agreed within 4% of Pandora retrieved TC NO₂ (Herman et al., 2009). Wang et al. (2010) showed that Pandora slant column abundances agree with those obtained from a multifunction differential optical absorption spectroscopy (DOAS) to within 5%. Validation results from the CINDI (Cabauw Intercomparison Campaign for Nitrogen Dioxide Measuring Instruments) campaign have also indicated that MAX-DOAS slant column densities of NO₂ from multiple instruments, including Pandora, have agreement of approximately 5–10% (Peters et al., 2012) under clear sky conditions. This measurement site of the CINDI campaign, Cabauw, the Netherlands, is similar to Welgegund in that it does not have major local sources of trace gases like NO₂ but rather is impacted from transported pollution being downwind of urban areas (i.e., Rotterdam, Netherlands).

Because of temporal and spatial sampling, Pandora TC NO₂ retrievals capture tropospheric NO₂ variability better than once daily satellite-retrieved TC NO₂ products (e.g., OMI; Herman et al., 2009; Reed et al., 2015; Tzortziou et al., 2015). For this analysis, we averaged Pandora Level 4 quality-controlled vertical TC NO₂ data over 15 min intervals to match the suggested data frequency for the gas analyzers (Table 1). Absolute error in Pandora retrievals is ± 0.1 Dobson units ($0.1 \text{ DU} \sim 2.69 \times 10^{15} \text{ molecules/cm}^2$), with a precision of about ± 0.01 DU in clear skies according to data documentation. Note this error grows with noise created by clouds in a given retrieval, such as the conditions observed during our 2011 Welgegund observing period. The Pandora data were filtered to only include data with uncertainty in TC NO₂ $< 0.05 \text{ DU}$ ($\sim 1.3 \times 10^{15} \text{ molecules/cm}^2$) for retrieval error and nonfunctioning periods and normalized root mean square of weighted spectral fitting residuals < 0.05 for cloud cover threshold exceedances as suggested by Herman et al. (2009) and Tzortziou et al. (2012). The filtered Pandora TC NO₂ retrievals have uncertainties of $\sim 7\%$ and $\sim 17\%$ during the Welgegund and DANCE campaigns, respectively (including both polluted and clean atmospheric conditions).

2.2.2. Ozone Monitoring Instrument

OMI, a near-UV/visible charged-coupled device nadir-viewing spectrometer, was launched on the NASA EOS Aura satellite in July 2004 and crosses the equator between 13:40 and 13:50 local time every day as a part of the A-Train satellite constellation (Boersma et al., 2007; L'Ecuyer & Jiang, 2010; Levelt et al., 2006; Schoeberl et al., 2006). OMI measurements cover a spectral range of 264–504 nm and provide retrievals with a spatial resolution of 13–26 km along and 24–128 km across track, achieving daily global coverage (every 2 days) of several trace gases, which include O₃, NO₂, SO₂, and HCHO. The OMI Level 2 version 3 (OMNO2-L2) retrieval algorithm uses a DOAS fit to calculate the slant column amount of NO₂ (Bucsela et al., 2006, 2013). Vertical TC NO₂ amounts are determined from the slant column abundances using air mass factors (AMFs), which are affected by both cloud cover and aerosols. Reed et al. (2015) demonstrated the effect of aerosols on OMI NO₂ column observations in urban and rural environments of the Baltimore/Washington, DC region, recognizing aerosols as a large source of error in AMFs. A monthly mean climatology of NO₂ profile shapes from the Global Modeling Initiative Chemical Transport Model (Strahan et al., 2007) accounts vertical variability in NO₂ in the retrieval algorithm (Boersma et al., 2002; Bucsela et al., 2006, 2013; Lamsal et al., 2014).

We use total, tropospheric, and stratospheric column NO₂ from the standard OMNO2-L2 data product available at the NASA GES DISC (Goddard Earth Sciences Data and Information Services Center; http://disc.sci.gsfc.nasa.gov/Aura/data-holdings/OMI/omno2_v003.shtml). Uncertainties in the tropospheric NO₂ columns (TropNO2) arise from the uncertainties in the retrieval of the slant column abundances, AMF calculations, and the separation of stratospheric and troposphere columns. The total expected error, dominated by AMF uncertainties over continental polluted regions, is $< 20\%$ for clear skies and 30–80% under cloudy conditions (Dobber et al., 2008). OMNO2-L2 data files include variables such as Cloudfraction and XTrackQualityFlag that are used for filtering and quality control. We selected retrievals in all cross track positions with cloud fractions $< 20\%$ and within 100 km of the Welgegund station or the ship track in the Atlantic. We also accounted for the “Row Anomaly” with XTrackQualityFlag = 0; this is a marker for Level 1B OMI radiances that are compromised by high signal-to-noise ratios due to limitations of the detector (Dobber et al., 2008). Figure 2 is an example of OMI TropNO2 abundances over South Africa on 10 March 2011 (day with minimal cloud coverage), indicating hotspot values $> 10 \times 10^{15} \text{ molec/cm}^2$ within the J-P megacity. A map of OMI TC NO₂ during DANCE is shown in Figure 3.

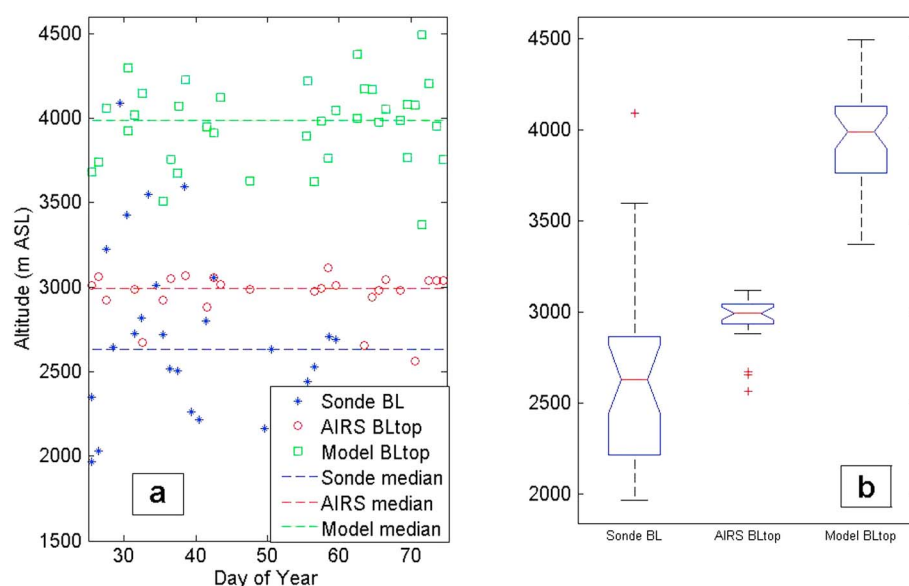


Figure 4. (a) Time series of PBL heights in meters ASL for AIRS (red), model (green), and radiosondes (blue) at Welgegund for OMI overpasses over the study period. (b) Box-and-whiskers plot of sonde, AIRS, and model PBL heights show the minimum (lower black dashes), 25th percentile (lower blue line), median (red line), 75th percentile (upper blue line), maximum daily values (upper black dashes), and outliers (red plus signs) for the entire Welgegund campaign.

As a result of weather conditions (i.e., rain and cloud cover) at the Welgegund station between 25 January and 15 March 2011, only 22 days of observations (satellite and ground) could be used for our comparisons based on the quality controls outlined. For the DANCE case study, the Knepp–Kollonige method could be applied to only 8 days of observations of the total 17 day campaign. Each day an average TC abundance of NO_2 was used for the area surrounding the site. Because a Pandora was located at either “ground” location, Welgegund site, or on board the ship during DANCE, OMI retrievals within 100 km or $\sim 1^\circ$ were collected. A mean TC was then calculated from those retrievals for a direct comparison to the Pandora TC.

2.3. Planetary Boundary Layer Height Variability

The estimation of surface mixing ratios from tropospheric column abundances depends on the daily variability of the PBL, which changes throughout the day, responding to local surface heating and synoptic meteorology. Based on Korhonen et al. (2014), where PBL tops showed good correlation with satellite and modeled observations at a measurement site (Elandsfontein) near J-P in the Mpumalanga industrial Highveld of South Africa, we selected both modeled and observed PBL heights for the analysis at Welgegund (Figure 4). Because PBL heights were not directly measured at the Welgegund site, we used three methods for calculating PBL heights: a model simulation, spatially and temporally co-located AIRS satellite observations, and observations from radiosonde launches at a nearby weather station. Each technique was considered for the column conversions; their respective observations are presented in Figure 4.

The first method used to determine PBL structure and evolution was a model simulation using Monin–Obukhov similarity theory. Inputs into the fifth generation Mesoscale Model (MM5) included hourly-averaged temperature, humidity, pressure, wind speed and direction, potential temperature gradient, global upwelling radiation, global incoming radiation and net radiation from the Welgegund measurement site, and NCEP reanalysis. Using the Hong and Pan (1996) boundary layer parameterization scheme, simulations provided hourly vertical temperature profile estimates. The hourly boundary layer height was derived similarly to Cimorelli et al. (2004) as used in the Aermid air dispersion regulatory model. For comparison to nearby observed PBL heights (Figure 4a), 1 h mean modeled PBL heights above sea level (ASL; green squares) within 1 h of the Aura overpass for days with Pandora and OMI measurements are presented for Welgegund.

Observations from the AIRS instrument, on board the NASA EOS Aqua satellite since 2002 and part of the A-Train satellite constellation, provide daily global observations within 15 min of the Aura satellite

(Aumann et al., 2003) and were collected for a second method of PBL height estimations. AIRS L2 V6 support files (described in http://disc.sci.gsfc.nasa.gov/AIRS/documentation/v6_docs/v6releasedocs-1/V6_L2_Product_User_Guide.pdf) contain a new product, PBL top, derived from temperature and humidity profiles with 100 levels via the method in Martins et al. (2010). The boundary layer top height is the pressure of the level with the largest gradients of potential temperature and relative humidity (relative to liquid phase of water) calculated on the support pressure 100 layer grid. Within the PBL, the data set has ~ 25 hPa vertical resolution and 45 km horizontal resolution (Susskind et al., 2006). AIRS quality control flags for PBL top are heavily dependent on the relative humidity and temperatures retrieved at the surface and throughout the lower troposphere (Martins et al., 2010; Susskind et al., 2010). Filtered AIRS retrievals were co-located temporally and spatially with the selected OMI retrievals for the surface NO_2 estimation method (Figure 4a, red circles) and compared to modeled PBL heights. The mean difference between 1,000 bootstrap samples of these two data sets is $\sim 30\%$ and statistically significant with 95% confidence (shown in Figure 4b).

In addition to model-derived and satellite-observed PBL heights, we also used radiosonde observations from a South African Weather Service station at Irene, 150 km northeast of Welgegund and at a similar elevation above sea level $\sim 1,500$ m, to determine an approximate height of the PBL for a similar environment. The radiosonde data were smoothed to 100 m resolution using a moving average filter. The World Meteorological Organization definition of the PBL top was calculated for simplicity (i.e., temperature gradient greater than 5 K/km). Radiosonde launches that corresponded in time with the Pandora and OMI observations (daytime overpass) numbered 16 out of the total 22 days. Figure 4a shows the calculated PBL heights from the radiosondes (blue stars). The median sonde-PBL height for the area near Welgegund is $\sim 2,700$ m ASL compared to $\sim 3,000$ m ASL and 4,000 m ASL for AIRS and the model, respectively (Figure 4b). This result suggests an approximate mixing layer depth of ~ 1.2 km measured from the sondes versus ~ 1.5 km as observed by AIRS. The mean difference between 1,000 bootstrap samples of the sonde-PBL and the AIRS-PBL is $\sim 11\%$. These PBL heights are consistent with recent ceilometer measurements at Welgegund (unpublished) ranging from ~ 1 to 2 km for $\sim 11:30$ UTC, the overpass time for Aura and Aqua.

PBL heights from the AIRS observations (within 100 km) were selected for the column conversions over Welgegund based on the better comparison with the sonde-PBL and for having at least once daily observations of the PBL. For DANCE, Martins et al. (2016) presented model-derived PBL heights ranging from ~ 160 to 950 m during the campaign time period. AIRS-observed PBL heights within the DANCE region ($34\text{--}39^\circ\text{N}$; $72\text{--}76^\circ\text{W}$) and time period are shown in Figure 5, and median values range between $\sim 1,000$ and 2,000 m ASL. This large difference between observations and simulations over ocean highlights the need for in situ PBL height measurements for validation. An infrared sensor, like AIRS, requires large thermal contrast between surface and atmosphere for strong signals. Over ocean, low signal strength contributes to higher retrieval errors and large variability in AIRS-observed PBL heights versus over land where signal strengths are higher (i.e., the Welgegund site). Due to no in situ ship PBL height measurements, the AIRS-observed values were selected for the DANCE surface estimation calculations to be consistent in using observations over model simulations and again provided similar data coverage with once daily daytime PBL heights.

2.4. Surface NO_2 Estimation, Knepp–Kollonige Method

NO_2 mixing ratios often display considerable vertical gradients within the PBL (Peters et al., 2012). The method for estimating surface NO_2 from a column amount developed by Knepp et al. (2015) assumes that surface emissions are well-mixed within the PBL as a first-order approximation (Leigh et al., 2007). To calculate Pandora Trop NO_2 densities, daily OMI stratospheric column NO_2 densities (using the OMNO2 version 3 L2 data) were resampled to the same temporal frequency as the quality-controlled Pandora measurements and subtracted from the Pandora TC NO_2 observations.

This method assumes that the NO_2 stratospheric column remains constant on a daily basis to simplify the calculation used to estimate surface mixing ratios. Also, this method assumes that most NO_2 in the troposphere is within the PBL, and the free troposphere contribution can be considered negligible under certain conditions. According to Lee et al. (2011), where surface NO_2 mixing ratios were inferred from OMI TCs over rural and suburban areas downwind of Detroit, MI, the free tropospheric contribution on average was 0.8×10^{15} molecules/cm² and smaller than most tropospheric columns even in the rural areas similar to

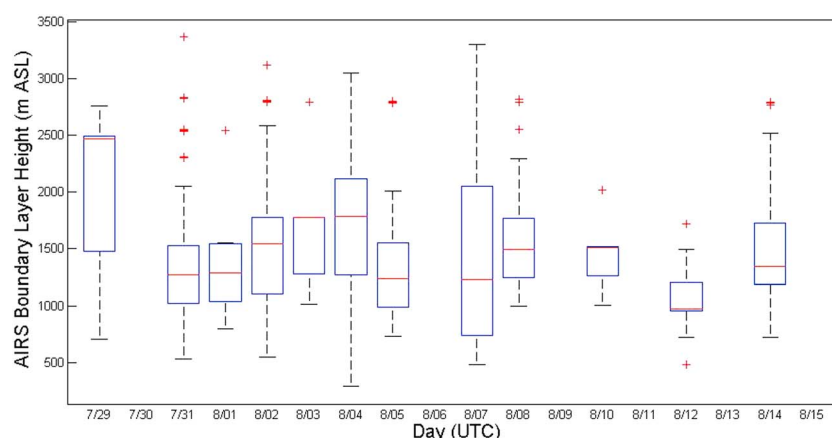


Figure 5. Box-and-whiskers plot of AIRS-observed PBL heights in meters ASL over the DANCE campaign show the minimum (lower black dashes), 25 percentile (lower blue line), median (red line), 75 percentile (upper blue line), maximum daily values (upper black dashes), and outliers (red plus signs).

our two locations. For our analysis, these conditions are most likely to occur if pollution transport is within the PBL or instabilities in the lower troposphere allow vertical transport of pollution layers toward the surface. The stratospheric contribution is significantly less than tropospheric column amount under polluted conditions, allowing for this assumption to work. This may break down in clean air conditions, such as a marine environment, so analysis was not completed at each site if stratospheric columns ($\sim 2 \times 10^{15}$ molecules/cm²) were close to or larger than the tropospheric column amounts to reduce the uncertainty this assumption adds to the estimated mixing ratios.

Pandora TropNO₂ is converted to mixing ratios, X_{Pan} , with equation (1):

$$X_{\text{Pan}}[\text{ppb}] = \frac{(\text{Pan}_{\text{col}} - \text{OMI}_{\text{strat}}) \times 1\text{E9}}{\text{PBL} \times N} \quad (1)$$

where Pan_{col} is the TC NO₂ measured by Pandora in molecules/cm², $\text{OMI}_{\text{strat}}$ is the OMI stratospheric component derived with its algorithm, PBL is the AIRS-observed value in centimeters coincident with Pandora observations, and N is the number density of air in molecules/cm³. This value, N , is determined from the in situ surface measurements because of its temperature and pressure dependence.

OMI-estimated surface NO₂ mixing ratios, X_{OMI} , are calculated with equation (2), which is similar to equation (1):

$$X_{\text{OMI}}[\text{ppb}] = \frac{(\text{OMI}_{\text{trop}}) \times 1\text{E9}}{\text{PBL} \times N} \quad (2)$$

where OMI_{trop} is the OMI tropospheric component derived in its algorithm in molecules/cm², PBL is the coincident AIRS-observed PBL top in centimeters, and N is the number density of air in molecules/cm³.

3. Results and Discussion

3.1. Pandora and OMI TC NO₂

When either the Pandora data or in situ data was selected to be co-located with OMI, the measurements were a ± 30 min mean value. The overpass time of OMI did vary (centered around 11:30 UTC), and the data were selected accordingly with the possibility of having more than one overpass. For Pandora comparisons at Welgegund, only three out of 22 days of observations had two overpasses for comparison (see Figure 6). For in situ versus OMI comparisons, this was also the case. For DANCE, data were selected similarly, and only one day of the 8 days of observations had more than one overpass.

To determine the temporal and spatial limitations of OMI for detecting NO₂ within the boundary layer over Welgegund, we first compared Pandora TC NO₂ measurements averaged over 1 h of the OMI overpass on 22 days, January 25 to 15 March 2011. OMI retrievals within 100 km (or $\sim 1^\circ$) were collected for each day, and a mean TC was calculated from those retrievals for a direct comparison to the corresponding Pandora

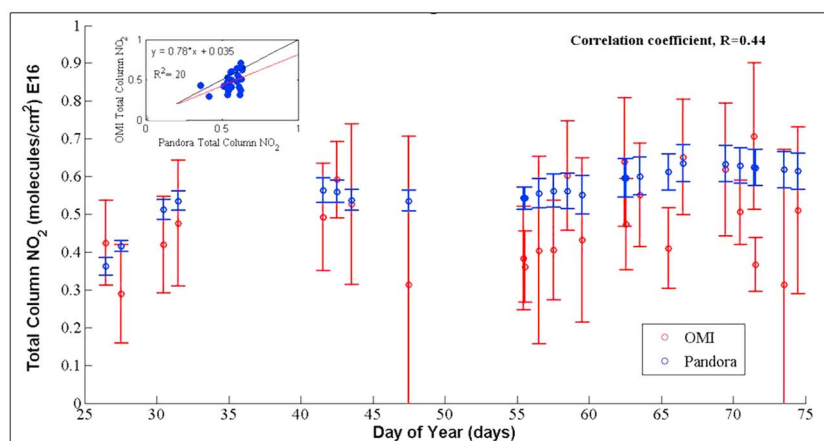


Figure 6. Total-column NO_2 for Pandora (blue) and OMI (red) at Welgegund, SA 25 January to 15 March 2011. Error bars represent an uncertainty of $\sim 7\%$ for Pandora and $\sim 35\%$ for OMI total column NO_2 . (inset) Pandora TC NO_2 and OMI TC NO_2 (blue points) in 10^{16} molecules/ cm^2 with a 1:1 line (black) and a linear fit (red line) with $R^2 = 0.20$.

TC amount. Figure 6 (and inset) shows a relatively good correlation with OMI TC NO_2 , that is, a correlation coefficient of $R = 0.44$ with a corresponding slope = 0.78, considering the rain and cloud cover during the campaign. The noise in the data, or uncertainties, in Figure 6 for the Pandora and OMI TC NO_2 measurements under the cloudy conditions we observed at Welgegund was $\sim 7\%$ and $\sim 35\%$, respectively. The difference between the two instruments was $\sim 20\%$, which is comparable to what Reed et al. (2015) determined for similar cloudy conditions.

In general, OMI observed lower TC NO_2 abundances than Pandora during the experiment, and the largest discrepancies occurred on the more polluted days with higher cloud cover over the area (see Figure 7 ground measurements of O_3 , NO_x , and NO). This result is consistent with areas impacted by strong (local or transported) pollution (Reed et al., 2015; Tzortziou et al., 2015). In particular, Pandora retrieved higher TC NO_2 over Welgegund on \sim days 27, 47, and 74 (Figure 6) when fresh pollution (high NO_x and low O_3) was measured by ground analyzers as shown in Figure 7. The coarse spatial resolution of the OMI retrievals contributes to reduced NO_2 values here. When relatively clean rural air is adjacent to relatively more polluted air within the same satellite-retrieved field of view, this can cause averaging of higher NO_2 concentrations with lower NO_2 concentrations. This effect may lead to systematic OMI underestimations. Multiple days also correspond to cloudy and rainy conditions, and this was most likely the cause for the largest differences between Pandora and OMI TC NO_2 . Cloud cover affects TC retrievals through misinterpretation of the depth of the column observed by the remote sensing instrument (i.e., difficult for OMI to see below clouds and Pandora to see above). OMI could not detect enhanced NO_2 beneath the clouds; both effects (coarse resolution and

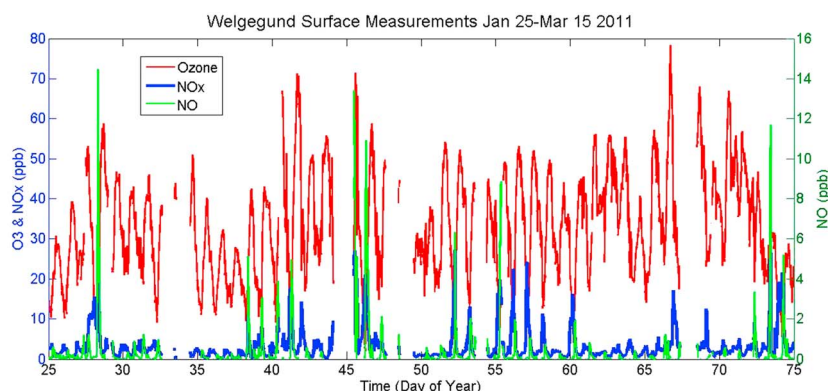


Figure 7. Surface O_3 (red), NO_x (blue), and NO (green) mixing ratios at Welgegund, 25 January to 15 March 2011.

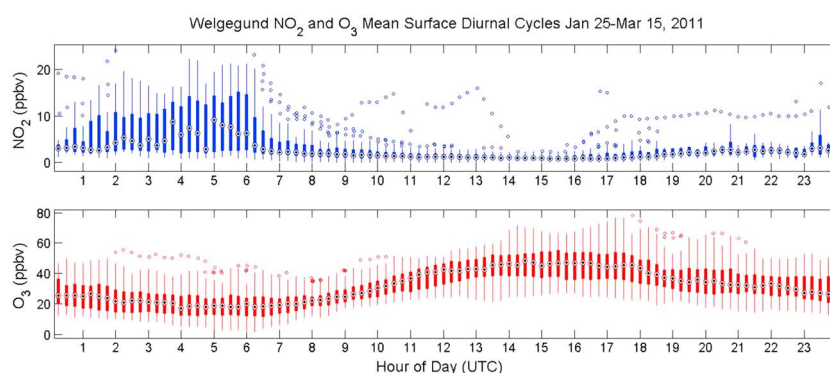


Figure 8. Diurnal cycles of surface in situ O_3 (red) and NO_2 (blue) as measured at the Welgegund site over the study period where black circles are the median, bars are the 25th and 75th percentiles, and open circles are the outliers for the respective species. OMI overpasses Welgegund at approximately 1:30 pm local time or 11:30 UTC.

cloud cover) lead to OMI underestimations. This limitation will result in low surface estimations of NO_2 from our OMI observations.

The diurnal cycle of NO_2 and O_3 measured at Welgegund for this time period is shown in Figure 8. Restricted by the once daily observations, OMI TCs cannot capture this variability like the Pandora instrument (Knepp et al., 2015). The highest surface NO_2 concentrations are observed earlier in the day (morning) before the Aura overpass of Welgegund at 11:30UTC. This denotes the importance of high temporal frequency measurements when discussing TC NO_2 variability, whether from a Pandora instrument or from upcoming geostationary missions.

Martins et al. (2016) presented comparisons between coincident and co-located OMI and Pandora-ship TC NO_2 on 8 days of DANCE observations. A total least squares fit between the data sets resulted in a slope = 0.46 and correlation coefficient of $R = 0.57$ with OMI overestimating in all but one data pair (data not shown here), which is common at nonurban sites (Reed et al., 2015; Tzortziou et al., 2015). Better correlation of the TC NO_2 abundances over ocean suggests the retrieval of similar columns unobstructed by cloud cover versus over Welgegund, where OMI retrieved a tropospheric column obstructed by clouds with the majority of NO_2 below the cloud cover on multiple days based on the surface and Pandora observations. However, the Welgegund campaign as a whole had a better 1:1 ratio of Pandora to OMI TC NO_2 abundances. During DANCE, Pandora TC NO_2 values (not shown) ranged from 0.1 to 0.3 DU (2.67×10^{15} – 8.01×10^{15} molecules/cm²), whereas at Welgegund, Pandora measured TC NO_2 values from 3×10^{15} molecules/cm² to greater than 1×10^{16} molecules/cm². This result can be attributed to more frequent NO_2 enhancements from nearby Highveld sources (and higher signal strengths) captured by both OMI and Pandora at the Welgegund site versus over clean marine air (only impacted once by downwind pollution transport from the mid-Atlantic U.S.).

3.2. Pandora-Estimations Compared to Surface NO_2

3.2.1. Welgegund Campaign

Pandora estimates of surface NO_2 at the Welgegund site were calculated using the Knepp–Kollonige method (equation (1) in section 2.4), where co-located and coincident AIRS-observed PBL heights, OMI stratospheric NO_2 columns, and number density (N) were resampled to the 15 min averaged Pandora time steps. Figure 9 presents a comparison between Pandora-estimated surface NO_2 mixing ratios and the in situ surface NO_2 mixing ratios at 15 min intervals. Pandora (green squares) generally agrees with the surface (blue stars) NO_2 concentrations (Figure 9a); estimates were mostly within the uncertainty limit of the gas analyzer ~50%. The mean NO_2 surface mixing ratio for this study as measured with the gas analyzer was 1.55 ppbv, while the Pandora-estimated surface mean was ~1.2 ppbv (a mean bias of ~20%). A reduced-major axis (RMA) fit between the two data sets (blue line in Figure 9b) resulted in a slope of 0.661. With PBL height as a major source of uncertainty, the resampling of daily AIRS observations to the Pandora time intervals will affect the Pandora-estimated surface mixing ratios.

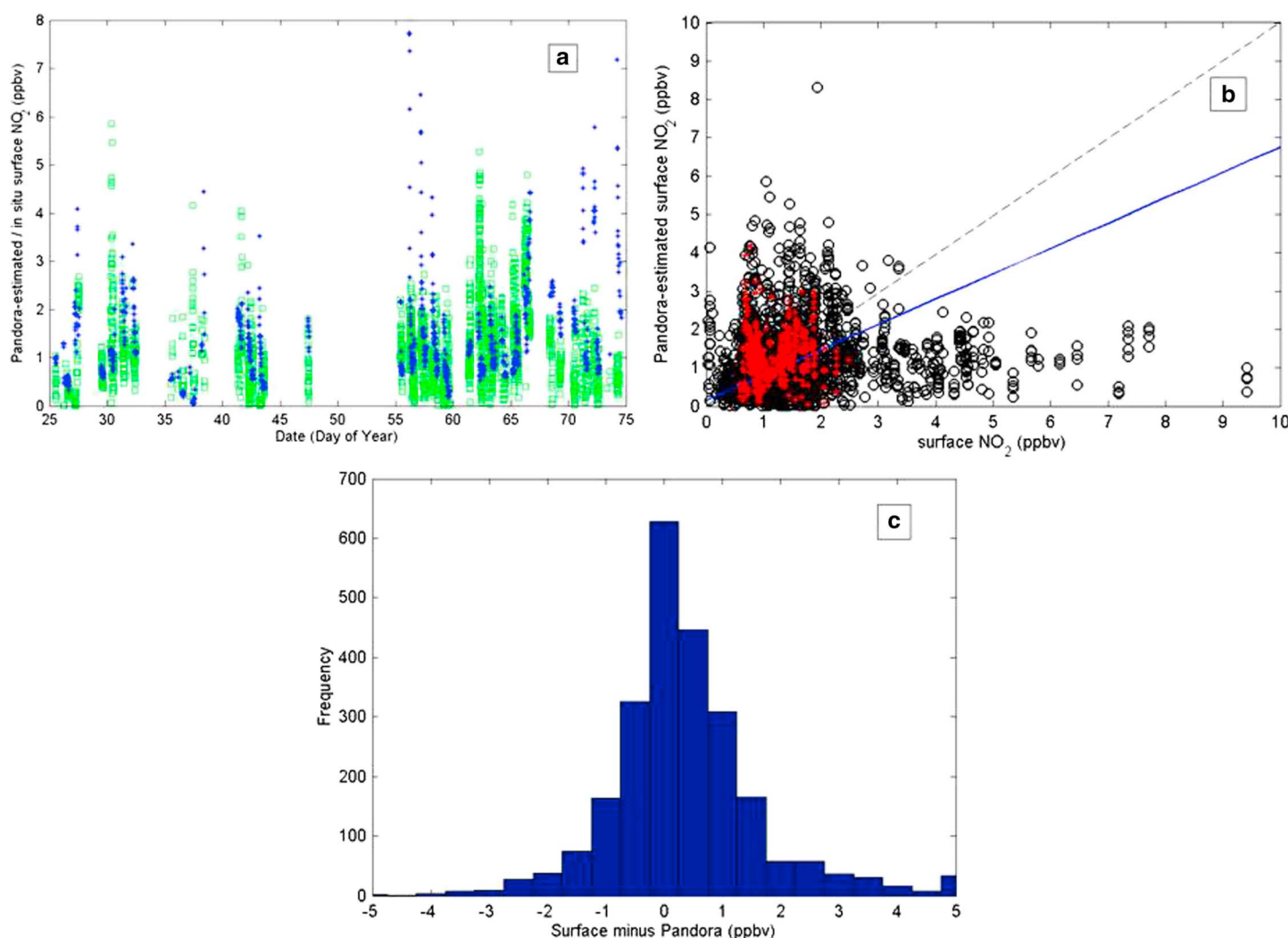


Figure 9. (a) Time series of Pandora-estimated (green squares) and in situ (blue stars) surface NO₂ for 25 January to 15 March 2011 at the Welgegund site. (b) Comparison between Pandora-estimated and in situ surface NO₂ (black dashed line 1:1 line, blue line RMA fit). Red stars denote days 63–65 of good agreement. (c) Histogram of differences (bin size = 0.5 ppbv).

A low correlation coefficient of $R = 0.10$ and the diurnal differences between the estimates and the in situ measurements (Figure 9a) may also be attributed to different sources of NO₂ at the ground site. If a pollution plume was advected over the Welgegund site with NO₂ aloft, Pandora may detect an enhancement in TC NO₂ before high concentrations of NO₂ were measured at the surface. Before any downward vertical mixing, Pandora estimates would peak before the surface in situ measurements (day 42, Figure 9a). On days 42–44, wind direction at the site suggests NO₂ most likely came from surrounding industrial sources to the northeast (Western Bushveld Igneous Complex) and southeast (Vaal Triangle). Conversely, if the source of NO₂ was local, any enhancements in NO₂ measured at the surface may be observed prior to Pandora detection unless convection was present. This effect could account for any temporal differences in the diurnal variability observed from Pandora and the surface monitor.

In Figure 9c, the histogram is centered on a 0–0.5 ppbv difference between the Pandora-estimated and in situ surface NO₂. The largest discrepancies between Pandora and the gas analyzer, where surface NO₂ was significantly underestimated by Pandora, fell on days 56–59 (25–28 February 2011) and days 71–74 (12–15 March 2011). During both time periods, NO₂ concentrations were enhanced at the surface (>5 ppbv; Figure 9a), but Pandora-estimated surface NO₂ mixing ratios were ~2 ppbv or less. Low clouds and intermittent rain in the region on days 56–59 likely impacted the Pandora TC NO₂ used in the calculation. For days 71–74, hard rain

and clouds also influenced Pandora-estimated surface NO_2 . In previous campaigns on the South African Highveld (i.e., SAFARI-1992), intense rainfall released NO from soil. In an agricultural environment like Welgegund, the soil can add NO emissions (thus NO_2) to the air that can be captured by the in situ instrument more easily under these weather conditions. These large differences between the ground measurements and Pandora could also be attributed to interference species measured by the gas analyzer using a molybdenum converter. In Piters et al. (2012), a comparison between this type of instrument and a photolytic converter found differences as large as 5 ppbv during the day time. The solar UV needed to generate these interfering species was still present on many of these days where rainfall was not constant the entire day. The group of outliers in Figure 9b where surface concentrations are much higher than those estimated from Pandora TC NO_2 could be directly related to the fact that this gas analyzer measures more than just NO_2 as compared to Pandora.

The only notable time period during which Pandora overestimated surface NO_2 in Figures 9a and 9b occurred on days 62–63 (3–4 March) when high clouds over the region affected the TC NO_2 retrievals. Pandora TropNO2, derived from Pandora TC NO_2 and daily OMI stratospheric columns, could be overestimated if the OMI retrieval had difficulty in separating the stratospheric and tropospheric column abundances in the presence of high clouds. This result suggests that OMIstrat ($\sim 2.5\text{--}3 \times 10^{15}$ molecules/cm²) could influence our estimations under those particular observed conditions, but this is only of importance under clean atmospheric conditions. The best agreement between the Pandora-estimated and ground site surface NO_2 measurements (Figure 9b denoted by red stars) followed after this time period (days 63–65; 4–6 March 2011), where their relationship was close to the 1:1 line in Figure 9b (black dashed line).

3.2.2. DANCE Campaign

Using the Knepp–Kollonige method, a similar analysis was completed over open water during the DANCE campaign with the onboard Pandora TC and in situ NO_2 ship observations. Co-located and coincident AIRS-observed PBL heights, OMI stratospheric NO_2 columns, and number density (N , calculated with in situ ship measurements) were interpolated to the 15 min averaged Pandora time steps. Eight days (out of 17 total days) of Pandora estimations and ship observations were compared and are presented in Figure 10.

The surface estimate of NO_2 using the Pandora data was largely underestimated (Figure 10a), assuming the in situ NO_2 measurements from the ship are true, with differences of ~ 3 ppbv or greater (higher than those observed at Welgegund). A RMA fit resulted in a slope of 0.0165 and a statistically significant low correlation coefficient of $R = 0.0818$ (Figure 10b) based on the bootstrap method using 10,000 samples. Pandora did observe a change in TC NO_2 initially, but missed most of the polluted days during DANCE (06–10 August) due to cloudy conditions, affecting the Knepp–Kollonige method; whereas this method demonstrated good performance at Welgegund, South Africa, with a mean bias less than 1 ppbv. The main source for error with the DANCE data set is attributed to the large variability and uncertainty associated with the AIRS-observed PBL heights (Figure 5) over water discussed in section 2.3. Overestimating PBL height leads to underestimating Pandora NO_2 mixing ratios due to their inverse relationship (equation (1)). This dependence appears to have a larger effect over a marine environment with shallow boundary layer heights and limited measurements versus a land site like Welgegund with typically higher PBL heights. Martins et al. (2016) showed that model PBL heights were not necessarily an improvement over the AIRS-observed PBL heights over water. Based on these results, we can conclude that without in situ PBL height measurements, estimates of surface NO_2 from Pandora TC NO_2 measurements over ocean are likely to be in error.

3.3. OMI Estimations Compared to Surface NO_2 Measurements

The remotely sensed (Pandora and OMI) TC data are sensitive and responsive to clear changes in boundary layer concentrations at Welgegund. For example, higher TC NO_2 abundances during late February and early March are consistent with the ground measurements of Figure 7, where more pollution (higher O_3 and NO_x concentrations) was measured after 11 February (day 42). This result was also captured by the Pandora estimates at Welgegund. However, the following results demonstrate the limited use of the Knepp–Kollonige method with OMI-like observations over land (i.e., Welgegund) and marine (i.e., DANCE) environments.

For the 22 days of coincident and co-located observations at Welgegund, OMI-estimated surface NO_2 levels using AIRS-observed PBL heights (from equation (2)) are compared to in situ surface measurements (Figure 11). Because OMI has only one to two overpasses per day (at $\sim 1:30$ pm local time or 11:30 UTC), a

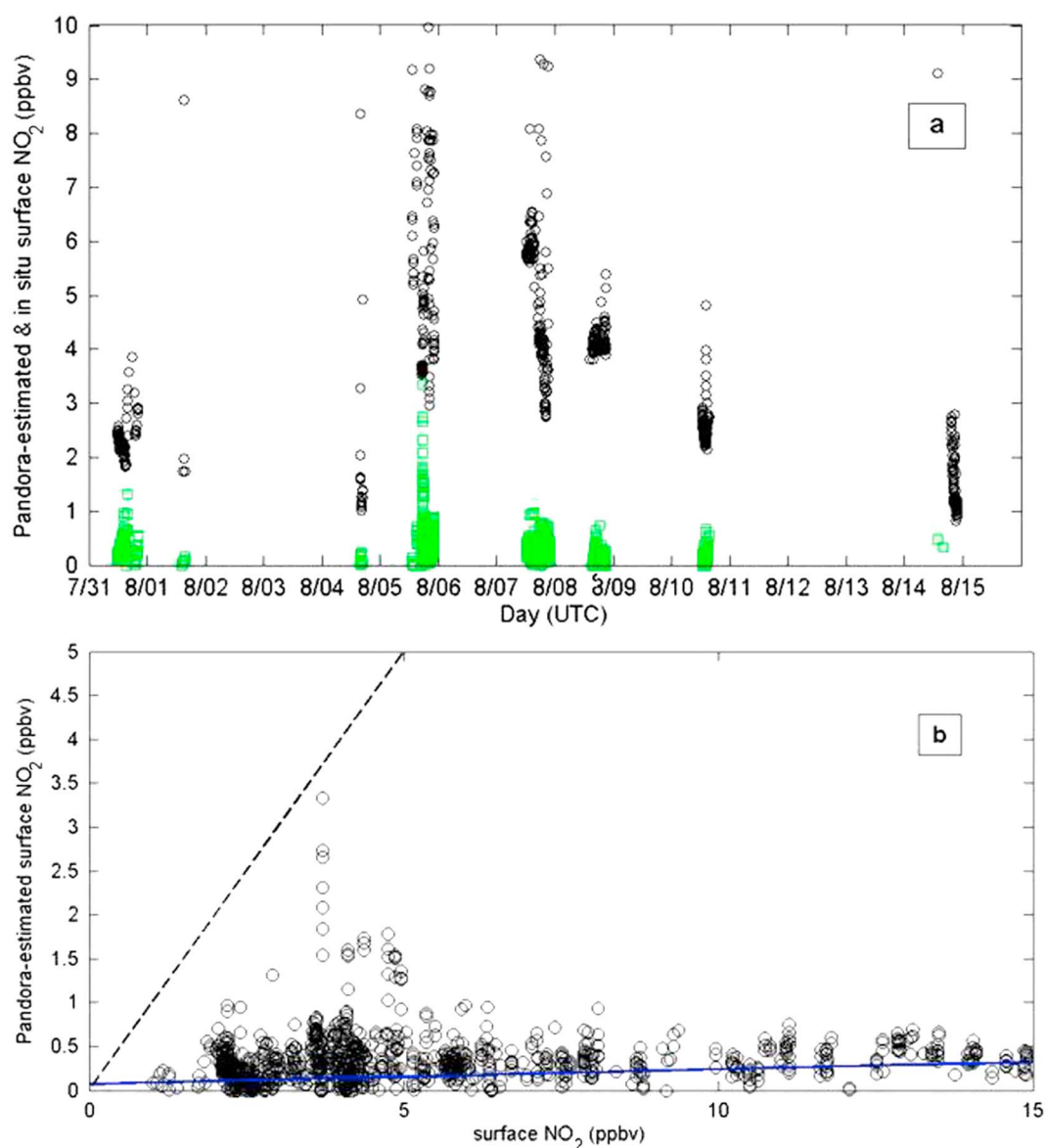


Figure 10. (a) Time series of Pandora-estimated (green diamonds) and in situ ship (black circles) surface NO₂ during the DANCE campaign in the North Atlantic Ocean. (b) Comparison between Pandora-estimated and ship surface NO₂ (black dashed line 1:1 line, blue line RMA fit).

direct comparison with the 15 min means of Pandora and the gas analyzer (in Figure 9) is not representative of the performance of this method applied to OMI observations. Diurnal cycles of surface NO₂ (top panel, blue) and O₃ (bottom panel, red) measured at the Welgegund site are presented in Figure 8. The time of day of the OMI overpass over Welgegund actually corresponds to a minimum in surface NO₂ concentrations, and the range of NO₂ concentrations is between 0 and 5 ppbv (not including outliers, open circles). By 1:30 pm (11:30 UTC), local photochemistry is dominant, and most of the NO₂ at the site has been lost to O₃ production (i.e., O₃ at a maximum concentration). For a better representation of the observed conditions at Welgegund, only mean surface NO₂ mixing ratios measured by the gas analyzer within 1 h of the OMI overpass are considered for a direct comparison to OMI-estimated surface NO₂.

A RMA fit of the OMI-estimated versus in situ surface NO₂ in Figure 11a indicates a slope of 0.225 and a statistically significant correlation coefficient of $R = 0.145$. Differences between the two data sets range between 0 and 4 ppbv (Figure 11b) with the most frequent as ~1 ppbv, which is larger than the bias of ~0.5 ppbv from

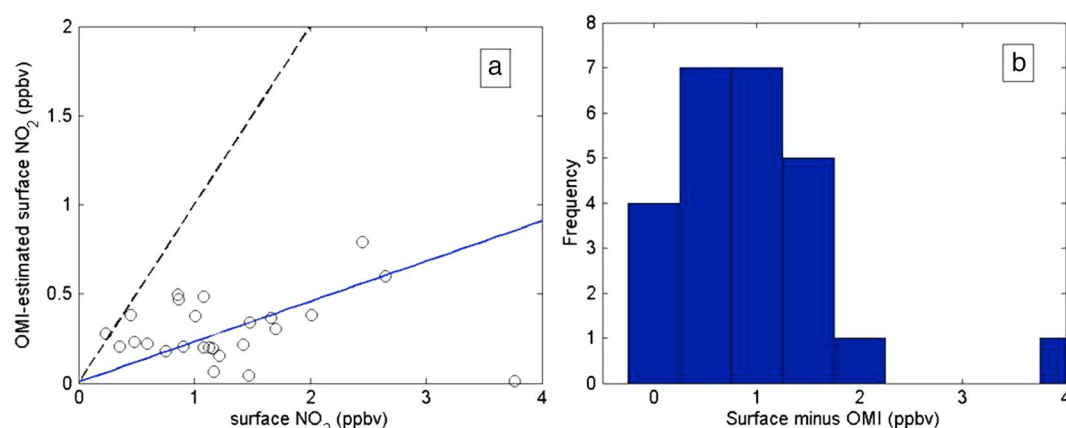


Figure 11. (a) Comparison between OMI-estimated and in situ surface NO₂ at Welgegund (black dashed line 1:1 line, blue line RMA fit). (b) Histogram of differences (bin size = 0.5ppbv).

Pandora estimates at Welgegund. The smallest differences evolved from favorable weather conditions. During March (days 66–75), the largest differences are a factor of 2 or more between the surface measurements and the OMI estimations (not shown). Rain and cloud cover during this time period affected the OMI retrievals and caused underestimates of the surface NO₂ concentration. Another reason for underestimations by OMI is the assumption that NO₂ is always evenly mixed in the PBL, a requirement for the conversion from TC to TropNO₂ with this method. This assumption is not always the case because fresh plumes might take a few hours to get to Welgegund from the nearest large point sources without mixing to the full height of the PBL.

The days where our OMI-estimated surface NO₂ compared well with the in situ measurements suggest that OMI is sensitive to boundary layer NO₂ over Welgegund. However, larger satellite signals (more urban than rural locations) of NO₂ under clear sky conditions would be best for this method when applied to satellite observations. This highlights the influence of cloudy versus clear sky conditions and related effects on the PBL. The effect of coarse spatial and temporal resolution is still problematic for OMI estimations, and new higher spatial resolution OMI products are being tested in future analyses with the Knepp–Kollonige method to determine any improvements.

For the DANCE campaign, the analysis was completed similarly to the Pandora estimates with the OMI tropospheric column NO₂ values instead. Limited coincidence and co-location between OMI and the in situ ship measurements (~10 data pairs) led to sparse OMI estimations. The differences between OMI-estimated surface NO₂ and the in situ ship measurements were mostly 3 ppbv or greater with OMI missing any NO₂ transport downwind during the pollution event. Typical OMI-estimated surface NO₂ was ~1 ppbv or less versus in situ values of ~3 ppbv or greater at overpass times. The results are not shown because differences were larger than the Pandora comparisons and can be attributed to similar effects that impacted the Pandora estimations discussed in section 3.2.2. In situ PBL heights would improve this method's performance over ocean versus using highly variable AIRS-observed PBL heights. The clean, source-free marine NO₂ amounts also approach the detection limit of the OMI instrument, which demonstrates the limitations of this method over water with the current generation of satellite instruments.

4. Summary and Conclusions

The first comparisons of total column NO₂ from a direct-Sun Pandora spectrometer located in South Africa (Welgegund site on the Highveld, southwest of the J-P conurbation) and over open ocean in the North Atlantic (DANCE campaign off the U.S. East Coast) are presented. Surface NO₂ mixing ratios estimated from Pandora and from OMI are compared to data from a co-located surface NO₂ analyzer at the land site, 25 January to 15 March 2011, and on the research vessel, 29 July to 15 August 2014, respectively. An adaptation of Knepp et al. (2015), Knepp–Kollonige method, has been used for deriving surface NO₂ values from OMI and Pandora for the comparison to surface NO₂ measured at both the terrestrial and marine environments.

With PBL height as a key variable in converting the column NO₂ amount to a surface value, the best PBL observations used in the estimations may vary. Of the three available approaches for calculating PBL height at Welgegund, two are in good agreement with an overall bias of ~10%: a new product, derived from AIRS observations; and PBL measured by radiosondes at Irene, 150 km northeast of Welgegund. This encouraging result appears to be one of the first evaluations of the AIRS-derived PBL product over land. During DANCE, however, the AIRS PBL product was the only available PBL observation, and no other comparisons could be made to determine performance over ocean.

The two main sources of error for the conversion of column to surface NO₂ are (1) poor weather conditions (e.g., cloud cover and precipitation) and (2) PBL height estimates, both affecting the NO₂ column–surface relationship and instrument sensitivities to boundary layer NO₂. Due to a higher-than-normal amount of cloud cover associated with a La Niña in early 2011, which results in higher than average rainfall in South Africa, only 22 days of observations are suitable for the Welgegund analysis. Nitrogen dioxide concentrations near J-P were sensitive to the weather conditions of a La Niña, as suggested by Balashov et al. (2014). Comparisons of coincidental, quality-controlled OMI and Pandora total column NO₂ show relatively good correlation (i.e., $R = 0.44$) with agreement of ~20%, comparable to previous studies under similar conditions. Absolute differences between Pandora-estimated surface NO₂ and the ground measurements are ~0.5 ppbv; however, OMI typically underestimated TC NO₂, causing estimates to be biased low by 1 ppbv or more. Pandora estimates compare moderately well with low percent differences, but a low correlation with the surface measurements ($R = 0.10$) demonstrates the influence of mixing within the PBL and the importance of the selected PBL height observations on the NO₂ column–surface relationship. Flynn et al. (2014) found similar results at sites with minimal local sources.

For the DANCE campaign, the Knepp–Kollonige method is less successful. The large variability in the co-located AIRS-derived PBL contributes to large differences between the Pandora and OMI estimates as compared to the in situ ship measurements. Additional PBL observations would have been required to determine fully the influence of this variable in the estimates. In addition, due to both Pandora and OMI encountering mostly clean marine air with NO₂ concentrations at or below background thresholds detectable by both instruments, their NO₂ estimates differ from in situ ship measurements by more than 3 ppbv. This difference suggests that estimates using this method are more reliable in environments with elevated NO₂ concentrations due to frequent pollution transport and/or local sources. To evaluate this method and hypothesis further, sites and/or more campaigns with longer time series and multiple PBL observations are necessary; we are examining other data for this purpose (i.e., DISCOVER-AQ campaign).

Estimating surface NO₂ from satellite observations, as we have demonstrated, can be a challenging problem. The temporal and spatial resolutions of observations from current instruments, such as OMI, add difficulty to the analysis and validation process when limited by few co-located observations over a single specific site. This emphasizes the need for instruments like TROPOMI, launched October 2017, with finer spatial observations and TEMPO (and other geostationary instruments) with higher temporal and spatial resolution for this type of air quality analysis. This work also indicates the need for the careful consideration of the location and coverage (i.e., networks) of ground-based instrumentation for validating satellites.

Acknowledgments

This research was funded through several NASA grants initially to Penn State University (AQUAST, NNG11AQ44G; Aura Validation, NNG05GO62G; SHADOZ, NNX09AJ23G) and also the National Science Foundation Division of Ocean Sciences (OCE 1260574) for the shipboard Pandora measurements. The deployment of Pandora at Welgegund was made possible by the hospitality of the North-West University—Potchefstroom and of a J. W. Fulbright Scholar award to A.M. Thompson. Data provided by OMI (doi: 10.5067/Aura/OMI/DATA2017) and AIRS (doi: 10.5067/AQUA/AIRS/DATA207) science teams are from NASA DISC. Irene data courtesy of an ongoing scientific collaboration with Gerrie Coetzee and the Observations Department from the South African Weather Service (SAWS) in conjunction with SHADOZ (Upper Air Research Program, K. W. Jucks). A special thank you to the Pandora team at GSFC for comments and recommendations on this work.

References

- Aumann, H. H., Chahine, M. T., Gautier, C., Goldberg, M. D., Kalnay, E., McMillin, L. M., ... Susskind, J. (2003). AIRS/AMSU/HSB on the aqua mission: Design, science objectives, data products, and processing systems. *IEEE Transactions on Geoscience and Remote Sensing*, 41(2), 253–264. <https://doi.org/10.1109/TGRS.2002.808356>
- Balashov, N. V., Thompson, A. M., Piketh, S. J., & Langerman, K. E. (2014). Surface ozone variability and trends over the South African Highveld from 1990 to 2007. *Journal of Geophysical Research: Atmospheres*, 119, 4323–4342. <https://doi.org/10.1002/2013JD020555>
- Beirle, S., Boersma, K. F., Platt, U., Lawrence, M. G., & Wagner, T. (2011). Megacity emissions and lifetimes of nitrogen oxides probed from space. *Science*, 333, 1737–1739. <https://doi.org/10.1126/science.1207824>
- Beukes, J. P., Vakkari, V., van Zyl, P. G., Venter, A. D., Josipovic, M., Jaars, K., ... Laakso, L. (2013). Source region plume characterisation of the interior of South Africa as observed at Welgegund. *Clean Air Journal*, 23(1).
- Beukes, J. P., Venter, A. D., Josipovic, M., Van Zyl, P. G., Vakkari, V., Jaars, K., ... Laakso, L. (2015). Chapter 6: Automated continuous air monitoring. In P. Forbes (Ed.), *Monitoring of Air Pollutants – Sampling, Sample Preparation and Analytical Techniques* (Vol. 70, pp. 183–208). Amsterdam, Netherlands: Elsevier. <https://doi.org/10.1016/bs.coac.2015.09.006>
- Boersma, K. F., Bucsela, E., Brinksma, E. J., & Gleason, J. F. (2002). NO₂. In K. Chance (Ed.), *OMI Algorithm Theoretical Basis Document, OMI Trace Gas Algorithms, ATBOMI-04, Version 2.0* (Vol. 4, pp. 13–36). Greenbelt, MD: NASA Data and Information Services Center.
- Boersma, K. F., Eskes, H. J., Veeffkind, J. P., Brinksma, E. J., van der A, R. J., Sneep, M., ... Bucsela, E. J. (2007). Near-real time retrieval of tropospheric NO₂ from OMI. *Atmospheric Chemistry and Physics*, 7, 2103–2118. <https://doi.org/10.5194/acp-7-2103-2007>

- Boersma, K. F., Jacob, D. J., Bucsela, E. J., Perring, A. E., Dirksen, R., van der A, R. J., ... Cohen, R. C. (2008). Validation of OMI tropospheric NO₂ observations during INTEX-B and application to constrain NO_x emissions over the eastern United States and Mexico. *Atmospheric Environment*, 42, 4480–4497. <https://doi.org/10.1016/j.atmosenv.2008.02.004>
- Boersma, K. F., Jacobs, D. J., Trancik, M., Rudich, Y., DeSmedt, I., Dirksen, R., & Eskes, H. J. (2009). Validation of urban NO₂ concentrations and their diurnal and seasonal variations observed from the SCIAMACHY and OMI sensors using in situ surface measurements in Israeli cities. *Atmospheric Chemistry and Physics*, 9, 3867–3879. <https://doi.org/10.5194/acp-9-3867-2009>
- Booyens, W., Van Zyl, P. G., Beukes, J. P., Ruiz-Jimenez, J., Kopperi, M., Riekkola, M.-L., ... Pienaar, J. J. (2015). Size-resolved characterisation of organic compounds in atmospheric aerosols collected at Welgegund, South Africa. *Journal of Atmospheric Chemistry*, 72(1), 43–64. <https://doi.org/10.1007/s10874-015-9304-6>
- Brauer, M., Amann, M., Burnett, R. T., Cohen, A., Dentener, F., Ezzati, M., ... Thurston, G. D. (2012). Exposure assessment for estimation of the global burden of disease attributable to outdoor air pollution. *Environmental Science & Technology*, 46, 652–660. <https://doi.org/10.1021/es2025752>
- Bucsela, E. J., Celarier, E. A., Wenig, M. O., Gleason, J. F., Veefkind, J. P., Boersma, K. F., & Brinksma, E. J. (2006). Algorithm for NO₂ vertical column retrieval from the ozone monitoring instrument. *IEEE Transactions on Geoscience and Remote Sensing*, 44, 1245–1258. <https://doi.org/10.1109/TGRS.2005.863715>
- Bucsela, E. J., Krotkov, N. A., Celarier, E. A., Lamsal, L. N., Swartz, W. H., Bhartia, P. K., ... Pickering, K. E. (2013). A new stratospheric and tropospheric NO₂ retrieval algorithm for nadir-viewing satellite instruments: Applications to OMI. *Atmospheric Measurement Techniques*, 6(10), 2607–2626. <https://doi.org/10.5194/amt-6-2607-2013>
- Burrows, J. P., Weber, M., Buchwitz, M., Rozanov, V., Ladstätter-Weissenmayer, A., Richter, A., ... Eisinger, M. (1999). The global ozone monitoring experiment (GOME): Mission concept and first scientific results. *Journal of the Atmospheric Sciences*, 56(2), 151–175. [https://doi.org/10.1175/1520-0469\(1999\)056%3C0151:TGOMEG%3E2.0.CO;2](https://doi.org/10.1175/1520-0469(1999)056%3C0151:TGOMEG%3E2.0.CO;2)
- Chai, T., Carmichael, G. R., Tang, Y., Sandu, A., Heckel, A., Richter, A., & Burrows, J. P. (2009). Regional NO_x emission inversion through a four-dimensional variational approach using SCIAMACHY tropospheric NO₂ column observation. *Atmospheric Environment*, 43, 5046–5055. <https://doi.org/10.1016/j.atmosenv.2009.06.052>
- Chance, K., Liu, X., Suleiman, R. M., Flittner, D. E., Al-Saadi, J., & Janz, S. J. (2013). Tropospheric emissions: Monitoring of pollution (TEMPO). Proc. SPIE 8866, Earth Observing Systems XVIII, 8866, 88660D-1–88660D-16. <https://doi.org/10.1117/12.2024479>
- Cimorelli, A. J., Perry, S. G., Venkatram, A., Weil, J. C., Paine, R. J., Wilson, R. B., ... Paumier, J. O. (2004). *AERMOD: Description of Model Formulation*. Research Triangle Park, NC: U. S. Environmental Protection Agency.
- Cosijn, C., & Tyson, P. D. (1996). Stable discontinuities in the atmosphere over South Africa. *South African Journal of Science*, 92, 381–386.
- Dobber, M. R., Kleipool, Q., Dirksen, R., Levelt, P. F., Jaross, G., Taylor, S., ... Rozemeijer, N. (2008). Validation of ozone monitoring instrument level 1b data products. *Journal of Geophysical Research*, 113, D15S06. <https://doi.org/10.1029/2007JD008665>
- Duncan, B. N., Lamsal, L. N., Thompson, A. M., Yoshida, Y., Lu, Z., Streets, D. G., ... Pickering, K. E. (2016). A space-based, high-resolution view of notable changes in urban NO_x pollution around the world (2005–2014). *Journal of Geophysical Research: Atmospheres*, 121, 976–996. <https://doi.org/10.1002/2015JD024121>
- Duncan, B. N., Prados, A. I., Lamsal, L., Liu, Y., Streets, D., Gupta, P., ... Ziemba, L. (2014). Satellite data of atmospheric pollution for U.S. air quality applications: Examples of applications, summary of data end-user resources, answers to FAQs, and common mistakes to avoid. *Atmospheric Environment*, 94, 647–662. <https://doi.org/10.1016/j.atmosenv.2014.05.061>
- Duncan, B. N., Yoshida, Y., de Foy, B., Lamsal, L. N., Streets, D., Lu, Z., ... Krotkov, N. A. (2013). The observed response of the ozone monitoring instrument (OMI) NO₂ column to NO_x emission controls on power plants in the United States: 2005–2011. *Atmospheric Environment*, 81, 102–111. <https://doi.org/10.1016/j.atmosenv.2013.08.068>
- Duncan, B. N., Yoshida, Y., Olson, J. R., Sillman, S., Martin, R. V., Lamsal, L., ... Crawford, J. H. (2010). Application of OMI observations to a space-based indicator of NO_x and VOC controls on surface ozone formation. *Atmospheric Environment*, 44, 2213–2223. <https://doi.org/10.1016/j.atmosenv.2010.03.010>
- Dunlea, E. J., Herndon, S. C., Nelson, D. D., Volkamer, R. M., San Martini, F., Sheehy, P. M., ... Molina, M. J. (2007). Evaluation of nitrogen dioxide chemiluminescence monitors in a polluted urban environment. *Atmospheric Chemistry and Physics*, 7, 2691–2704. <https://doi.org/10.5194/acp-7-2691-2007>
- Fishman, J., Al-Saadi, J. A., Creilson, J. K., Bowman, K. W., Burrows, J. P., Richter, A., ... Thompson, A. M. (2008). Remote sensing of tropospheric pollution from space. *Bulletin of the American Meteorological Society*, 89, 805–821. <https://doi.org/10.1175/2008BAMS2526.1>
- Fishman, J., Iraci, L. T., Al-Saadi, J., Chance, K., Chavez, F., Chin, M., ... Wang, M. (2012). The United States' next generation of atmospheric composition and coastal ecosystem measurements: NASA's geostationary coastal and air pollution events (GEO-CAPE) mission. *Bulletin of the American Meteorological Society*, 93, 1547–1566. <https://doi.org/10.1175/bams-d-11-00201.1>
- Flynn, C. M., Pickering, K. E., Crawford, J. H., Lamsal, L., Krotkov, N., Herman, J., ... Brent, L. (2014). Relationship between column-density and surface mixing ratio: Statistical analysis of O₃ and NO₂ data from the July 2011 Maryland DISCOVER-AQ mission. *Atmospheric Environment*, 92, 429–441. <https://doi.org/10.1016/j.atmosenv.2014.04.041>
- Freiman, M. T., & Piketh, S. J. (2003). Air transport into and out of the industrial Highveld region of South Africa. *Journal of Applied Meteorology*, 42(7), 994–1002. <https://doi.org/10.1175/15200450>
- Freiman, M. T., & Tyson, P. D. (2000). The thermodynamic structure of the atmosphere over South Africa: Implications for water vapour transport. *Water SA*, 26(2), 153–158. Retrieved from <http://www.wrc.org.za>
- Garstang, M., Tyson, P. D., Swap, R., Edwards, M., Källberg, P., & Lindsay, J. A. (1996). Horizontal and vertical transport of air over southern Africa. *Journal of Geophysical Research*, 101(D19), 23,721–23,736. <https://doi.org/10.1029/95JD00844>
- Giannakaki, E., Pfüller, A., Korhonen, K., Mielonen, T., Laakso, L., Vakkari, V., ... Komppula, M. (2015). One year of Raman lidar observations of free-tropospheric aerosol layers over South Africa. *Atmospheric Chemistry and Physics*, 15(10), 5429–5442. <https://doi.org/10.5194/acp-15-5429-2015>
- Grosjean, D., & Harrison, J. (1985). Response of chemi-luminescence NO_x analyzers and ultraviolet ozone analyzers to organic air-pollutants. *Environmental Science & Technology*, 19(9), 862–865. <https://doi.org/10.1021/es00139a016>
- Halla, J. D., Wagner, T., Beirle, S., Brook, J. R., Hayden, K. L., O'Brien, J. M., ... McLaren, R. (2011). Determination of tropospheric vertical columns of NO₂ and aerosol optical properties in a rural setting using MAX-DOAS. *Atmospheric Chemistry and Physics*, 11, 12,475–12,498. <https://doi.org/10.5194/acp-11-12475-2011>
- He, H., Stehr, J. W., Hains, J. C., Krask, D. J., Doddridge, B. G., Vinnikov, K. Y., ... Dickerson, R. R. (2013). Trends in emissions and concentrations of air pollutants in the lower troposphere in the Baltimore/Washington airshed from 1997 to 2011. *Atmospheric Chemistry and Physics*, 13, 7859–7874. <https://doi.org/10.5194/acp-13-7859-2013>

- Herman, J., Cede, A., Spinei, E., Mount, G., Tzortziou, M., & Abuhassan, N. (2009). NO₂ column amounts from ground-based Pandora and MFOAS spectrometers using the direct-Sun DOAS technique: Intercomparisons and application to OMI validation. *Journal of Geophysical Research*, 114, D13307. <https://doi.org/10.1029/2009JD011848>.
- Hilboll, A., Richter, A., & Burrows, J. P. (2013). Long-term changes of tropospheric NO₂ over megacities derived from multiple satellite instruments. *Atmospheric Chemistry and Physics*, 13(8), 4145–4169. <https://doi.org/10.5194/acp-13-4145-2013>
- Hong, S.-Y., & Pan, H.-L. (1996). Nonlocal boundary layer vertical diffusion in a medium-range forecast model. *Monthly Weather Review*, 124(10), 2322–2339. [https://doi.org/10.1175/1520-0493\(1996\)124%3C2322:NBLVDI%3E2.0.CO;2](https://doi.org/10.1175/1520-0493(1996)124%3C2322:NBLVDI%3E2.0.CO;2)
- Ingmann, P., Veihelmann, B., Langen, J., Lamarre, D., Stark, H., & Courrèges-Lacoste, G. B. (2012). Requirements for the GMES atmosphere service and ESA's implementation concept: Sentinels-4/-5 and -5p. *Remote Sensing of Environment*, 120, 58–69. <https://doi.org/10.1016/j.rse.2012.01.023>
- Jaars, K., Beukes, J. P., Van Zyl, P. G., Venter, A. D., Josipovic, M., Pienaar, J. J., ... Hakola, H. (2014). Ambient aromatic hydrocarbon measurements at Welgegund, South Africa. *Atmospheric Chemistry and Physics*, 14(13), 7075–7089. <https://doi.org/10.5194/acp-14-7075-2014>
- Jaars, K., Van Zyl, P. G., Beukes, J. P., Hellén, H., Vakkari, V., Josipovic, M., ... Hakola, H. (2016). Measurements of biogenic volatile organic compounds at a grazed savannah–grassland–agriculture landscape in South Africa. *Atmospheric Chemistry and Physics*, 16(24), 15,665–15,688. <https://doi.org/10.5194/acp-16-15665-2016>
- Kim, J. (2012). *GEMS (geostationary Environment Monitoring Spectrometer) Onboard the GeoKOMPSAT to Monitor Air Quality in High Temporal and Spatial Resolution Over Asia-Pacific Region*. In A. Abbasi & N. Giesen (Eds.) *EGU General Assembly Conference Abstracts* (Vol. 14, p. 4051) Copernicus Geophysical Research Abstracts, 22–27 April 2012, Vienna, Austria. Retrieved from <http://meetingorganizer.copernicus.org/EGU2012/EGU2012-4051.pdf>
- Kim, S.-W., Heckel, A., McKeen, S., Frost, G., Hsie, E.-Y., Trainer, M., ... Grell, G. (2006). Satellite-observed U.S. power plant NO_x emission reductions their impact on air quality. *Geophysical Research Letters*, 33, L22812. <https://doi.org/10.1029/2006GL027749s>.
- Knepp, T., Pippin, M., Crawford, J., Chen, G., Szykman, J., Long, R., ... Neil, D. (2015). Estimating surface NO₂ and SO₂ mixing ratios from fast-response total column observations and potential application to geostationary missions. *Journal of Atmospheric Chemistry*, 72(3–4), 261–286. <https://doi.org/10.1007/s10874-013-9257-6>
- Korhonen, K., Giannakaki, E., Mielonen, T., Pfüller, A., Laakso, L., Vakkari, V., ... Komppula, M. (2014). Atmospheric boundary layer top height in South Africa: Measurements with lidar and radiosonde compared to three atmospheric models. *Atmospheric Chemistry and Physics*, 14(8), 4263–4278. <https://doi.org/10.5194/acp-14-4263-2014>
- Laakso, L., Laakso, H., Aalto, P. P., Keronen, P., Petäjä, T., Nieminen, T., ... Kerminen, V.-M. (2008). Basic characteristics of atmospheric particles, trace gases and meteorology in a relatively clean southern African savannah environment. *Atmospheric Chemistry and Physics*, 8(16), 4823–4839. <https://doi.org/10.5194/acp-8-4823-2008>
- Laakso, L., Vakkari, V., Virkkula, A., Laakso, H., Backman, J., Kulmala, M., ... Kerminen, V.-M. (2012). South African EUCAARI measurements: Seasonal variation of trace gases and aerosol optical properties. *Atmospheric Chemistry and Physics*, 12, 1847–1864. <https://doi.org/10.5194/acp-12-1847-2012>
- Lamsal, L. N., Duncan, B. N., Yoshida, Y., Krotkov, N. A., Pickering, K. E., Streets, D. G., & Lu, Z. (2015). U. S. NO₂ trends (2005–2013): EPA air quality system (AQS) data versus improved observations from the ozone monitoring instrument (OMI). *Atmospheric Environment*, 110, 130–143. <https://doi.org/10.1016/j.atmosenv.2015.03.055>
- Lamsal, L. N., Krotkov, N. A., Celarier, E. A., Swartz, W. H., Pickering, K. E., Bucsela, E. J., ... Knepp, T. N. (2014). Evaluation of OMI operational standard NO₂ column retrievals using in situ and surface-based NO₂ observations. *Atmospheric Chemistry and Physics*, 14(21), 11,587–11,609. <https://doi.org/10.5194/acp-14-11587-2014>
- Lamsal, L. N., Martin, R. V., Padmanabhan, A., van Donkelaar, A., Zhang, Q., Sioris, C. E., ... Newchurch, M. J. (2011). Application of satellite observations for timely updates to global anthropogenic NO_x emission inventories. *Geophysical Research Letters*, 38, L05810. <https://doi.org/10.1029/2010GL046476>
- Lamsal, L. N., Martin, R. V., van Donkelaar, A., Celarier, E. A., Bucsela, E. J., Boersma, K. F., ... Wang, Y. (2010). In direct validation of tropospheric nitrogen dioxide retrieved from the OMI satellite instrument: Insight into the seasonal variation of nitrogen oxides at northern midlatitudes. *Journal of Geophysical Research*, 115, D05302. <https://doi.org/10.1029/2009JD013351>
- Lamsal, L. N., Martin, R. V., van Donkelaar, A., Steinbacher, M., Celarier, E. A., Bucsela, E., ... Pinto, J. P. (2008). Ground-level nitrogen dioxide concentrations inferred from the satellite-borne ozone monitoring instrument. *Journal of Geophysical Research*, 113, D16308. <https://doi.org/10.1029/2007JD009235>
- L'Ecuyer, T. S., & Jiang, J. H. (2010). Touring the atmosphere aboard the A-Train. *Physics Today*, 63, 36–41. <https://doi.org/10.1063/1.3463626>
- Lee, C. J., Brook, J. R., Evans, G. J., Martin, R. V., & Mihele, C. (2011). Novel application of satellite and in-situ measurements to map surface-level NO₂ in the Great Lakes region. *Atmospheric Chemistry and Physics*, 11, 11,761–11,775. <https://doi.org/10.5194/acp-11-11761-2011>
- Leigh, R. J., Corlett, G. K., Frieß, U., & Monks, P. S. (2007). Spatially resolved measurements of nitrogen dioxide in an urban environment using concurrent multi-axis differential optical absorption spectroscopy. *Atmospheric Chemistry and Physics*, 7(18), 4751–4762. <https://doi.org/10.5194/acp-7-4751-2007>
- Levelt, P. F., van den Oord, G. H. J., Dobber, M. R., Mälkki, A., Visser, H., de Vries, J., ... Saari, H. (2006). The ozone monitoring instrument. *IEEE Transactions on Geoscience and Remote Sensing*, 44, 1093–1101. <https://doi.org/10.1109/TGRS.2006.872333>
- Lourens, A. S., Beukes, J. P., van Zyl, P. G., Fourie, G., Burger, J., Pienaar, J. J., ... Jordan, J. H. L. (2011). Spatial and temporal assessment of gaseous pollutants in the Highveld of South Africa. *South African Journal of Science*, 107, 269, 8. <https://doi.org/10.4102/sajs.v107i1/2.269>
- Lourens, A. S., Butler, T., Beukes, J. P., van Zyl, P. G., Steffen, B., Wagner, T., ... Lawrence, M. G. (2012). Re-evaluating the NO₂ hotspot over the South African Highveld. *South African Journal of Science*, 108, 1146. <https://doi.org/10.4102/sajs.v108i11/12.1146>
- Loyola, D. G., Gimeno García, S., Lutz, R., Romahn, F., Spurr, R. J. D., Pedernana, M., ... Schüssler, O. (2017). The operational cloud retrieval algorithms from TROPOMI on board Sentinel-5 precursor. *Atmospheric Measurement Techniques Discussions*, 1–30. <https://doi.org/10.5194/amt-2017-128>
- Lu, Z., & Streets, D. G. (2012). Increase in NO_x emissions from Indian thermal power plants during 1996–2010: Unit-based inventories and multisatellite observations. *Environmental Science & Technology*, 46, 7463–7470. <https://doi.org/10.1021/es300831w>
- Luo, Y. H., Sun, L. G., Liu, W. Q., Xie, P. H., Si, F. Q., & Zhou, H. J. (2012). MAX-DOAS measurements of NO₂ column densities and vertical distribution at Ny-Ålesund, Arctic during summer. *Spectroscopy and Spectral Analysis*, 32(12), 3363–3366. [https://doi.org/10.3964/j.issn.1000-0593\(2012\)09-2336-05](https://doi.org/10.3964/j.issn.1000-0593(2012)09-2336-05)
- Martin, R. V. (2008). Satellite remote sensing of surface air quality. *Atmospheric Environment*, 42, 7823–7843. <https://doi.org/10.1016/j.atmosenv.2008.07.018>

- Martins, D. K., Najjar, R. G., Tzortziou, M., Abuhassan, N., Thompson, A. M., & Kollonige, D. E. (2016). Spatial and temporal variability of ground and satellite column measurements of NO₂ and O₃ over the Atlantic Ocean during the deposition of atmospheric nitrogen to coastal ecosystems experiment (DANCE). *Journal of Geophysical Research*, 121(23), 14,175–14,187. <https://doi.org/10.1002/2016JD024998>
- Martins, J. P. A., Teixeira, J., Soares, P. M. M., Miranda, P. M. A., Kahn, B. H., Dang, V. T., ... Fishbein, E. (2010). Infrared sounding of the trade-wind boundary layer: AIRS and the RICO experiment. *Geophysical Research Letters*, 37, L24806. <https://doi.org/10.1029/2010GL045902>
- Newell, R. E., Thouret, V., Cho, J. Y. N., Stoller, P., Marengo, A., & Smit, H. G. (1999). Ubiquity of quasi-horizontal layers in the troposphere. *Nature*, 398(6725), 316–319. <https://doi.org/10.1038/18642>
- Petäjä, T., Vakkari, V., Pohja, T., Nieminen, T., Laakso, H., Aalto, P. P., ... Laakso, L. (2013). Transportable aerosol characterisation trailer with trace gas chemistry: Design, instruments and verification. *Aerosol and Air Quality Research*, 13, 421–435.
- Petrìoli, A., Bonasoni, P., Giovanelli, G., Ravegnani, F., Kostadinov, I., Bortoli, D., ... Fortezza, P. (2004). First comparison between ground-based and satellite-borne measurements of tropospheric nitrogen dioxide in the Po basin. *Journal of Geophysical Research*, 109, D15307. <https://doi.org/10.1029/2004JD004547>
- Peters, A. J. M., Boersma, K. F., Kroon, M., Hains, J. C., Van Roozendaal, M., Wittrock, F., ... Zhou, Y. (2012). The Cabauw intercomparison campaign for nitrogen dioxide measuring instruments (CINDI): Design, execution, and early results. *Atmospheric Measurement Techniques*, 5, 457–485. <https://doi.org/10.5194/amt-5-457-2012>
- Reay, D. S., Dentener, F., Smith, P., Grace, J., & Feely, R. A. (2008). Global nitrogen deposition and carbon sinks. *Nature Geoscience*, 1, 430–437.
- Reed, A. J., Thompson, A. M., Kollonige, D. E., Martins, D. K., Tzortziou, M. A., Herman, J. R., ... Cede, A. (2015). Effects of local meteorology and aerosols on ozone and nitrogen dioxide retrievals from OMI and Pandora spectrometers in Maryland, USA during DISCOVER-AQ 2011. *Journal of Atmospheric Chemistry*, 72(3–4), 455–482. <https://doi.org/10.1007/s10874-013-9254-9>
- Russell, A. R., Valin, L. C., & Cohen, R. C. (2012). Trends in OMI NO₂ observations over the United States: Effects of emission control technology and the economic recession. *Atmospheric Chemistry and Physics*, 12, 12,197–12,209. <https://doi.org/10.5194/acp-12-12197-2012>
- Schoeberl, M. R., Douglass, A. R., Hilsenrath, E., Bhartia, P. K., Beer, R., Waters, J. W., ... DeCola, P. (2006). Overview of the EOS aura mission. *IEEE Transactions on Geoscience and Remote Sensing*, 44, 1066–1074. <https://doi.org/10.1109/TGRS.2005.861950>
- Steinbacher, M., Zellweger, C., Schwarzenbach, B., Bugmann, S., Buchmann, B., Ordóñez, C., ... Hueglin, C. (2007). Nitrogen oxides measurements at rural sites in Switzerland: Bias of conventional measurement techniques. *Journal of Geophysical Research*, 112, D11307. <https://doi.org/10.1029/2006JD007971>
- Strahan, S. E., Duncan, B. N., & Hoor, P. (2007). Observationally derived transport diagnostics for the lowermost stratosphere and their application to the GMI chemistry and transport model. *Atmospheric Chemistry and Physics*, 7, 2435–2445. <https://doi.org/10.5194/acp-7-2435-2007>
- Streets, D., Canty, T., Carmichael, G., de Foy, B., Dickerson, R., Duncan, B., ... Wecht, K. (2013). Emissions estimation from satellite retrievals: A review of current capability. *Atmospheric Environment*, 77, 1011–1042. <https://doi.org/10.1016/j.atmosenv.2013.05.051>
- Susskind, J., Barnet, C., Blaisdell, J., Iredell, L., Keita, F., Kouvaris, L., ... Chahine, M. (2006). Accuracy of geophysical parameters derived from atmospheric infrared sounder/advanced microwave sounding unit as a function of fractional cloud cover. *Journal of Geophysical Research*, 111, D09S17. <https://doi.org/10.1029/2005JD006272>
- Susskind, J., Blaisdell, J. M., Iredell, L., & Keita, F. (2010). Improved temperature sounding and quality control methodology using AIRS/AMSU data: The AIRS science team version 5 retrieval algorithm. *IEEE Transactions on Geoscience and Remote Sensing*, 49, 883–907. <https://doi.org/10.1109/TGRS.2010.2070508>
- Tiitta, P., Vakkari, V., Croteau, P., Beukes, J. P., van Zyl, P. G., Josipovic, M., ... Laakso, L. (2014). Chemical composition, main sources and temporal variability of PM₁ aerosols in southern African grassland. *Atmospheric Chemistry and Physics*, 14(4), 1909–1927. <https://doi.org/10.5194/acp-14-1909-2014>
- Tzortziou, M., Herman, J. R., Cede, A., & Abuhassan, N. (2012). High precision, absolute total column ozone measurements from the Pandora spectrometer system: Comparisons with data from a brewer double monochromator and Aura OMI. *Journal of Geophysical Research*, 117(D16), D16303. <https://doi.org/10.1029/2012JD017814>
- Tzortziou, M., Herman, J. R., Loughner, C. P., Cede, A., Abuhassan, N., & Naik, S. (2015). Spatial and temporal variability of ozone and nitrogen dioxide over a major urban estuarine ecosystem. *Journal of Atmospheric Chemistry*, 72(3–4), 287–309. <https://doi.org/10.1007/s10874-013-9255-8>
- Vakkari, V., Kerminen, V.-M., Beukes, J. P., Tiitta, P., Van Zyl, P. G., Josipovic, M., ... Laakso, L. (2014). Rapid changes in biomass burning aerosols by atmospheric oxidation. *Geophysical Research Letters*, 41(7), 2644–2651. <https://doi.org/10.1002/2014GL059396>
- van Donkelaar, A., Martin, R. V., Brauer, M., Kahn, R., Levy, R., Verduzco, C., & Villeneuve, P. J. (2010). Global estimates of ambient fine particulate matter concentrations from satellite-based aerosol optical depth: Development and application. *Environmental Health Perspectives*, 118(6), 847–855. <https://doi.org/10.1289/ehp.0901623>
- Venter, A. D., Beukes, J. P., Van Zyl, P. G., Josipovic, M., Jaars, K., & Vakkari, V. (2016). Regional atmospheric Cr(VI) pollution from the Bushveld complex, South Africa. *Atmospheric Pollution Research*, 7(5), 762–767. <https://doi.org/10.1016/j.apr.2016.03.009>
- Venter, A. D., Vakkari, V., Beukes, J. P., van Zyl, P. G., Laakso, H., Mabaso, D., ... Laakso, L. (2012). An air quality assessment in the industrialized western Bushveld igneous complex, South Africa. *South African Journal of Science*, 108, 1059. <https://doi.org/10.4102/sajs.v108i9/10.1059>
- Wang, S., Pongetti, T. J., Sander, S. P., Spinei, E., Mount, G. H., Cede, A., & Herman, J. (2010). Direct Sun Measurements of NO₂ column abundances from Table Mountain, California: Intercomparison of low-and high-resolution spectrometers. *Journal of Geophysical Research*, 115, D13305. <https://doi.org/10.1029/2009JD013503>
- Zoogman, P., Liu, X., Suleiman, R. M., Pennington, W. F., Flittner, D. E., Al-Saadi, J. A., ... Chance, K. (2017). Tropospheric emissions: Monitoring of pollution (TEMPO). *Journal of Quantitative Spectroscopy and Radiation Transfer*, 186, 17–39. <https://doi.org/10.1016/j.jqsrt.2016.05.008>